Resource

Developmental Cell

Live Tracking of Inter-organ Communication by Endogenous Exosomes *In Vivo*

Graphical Abstract

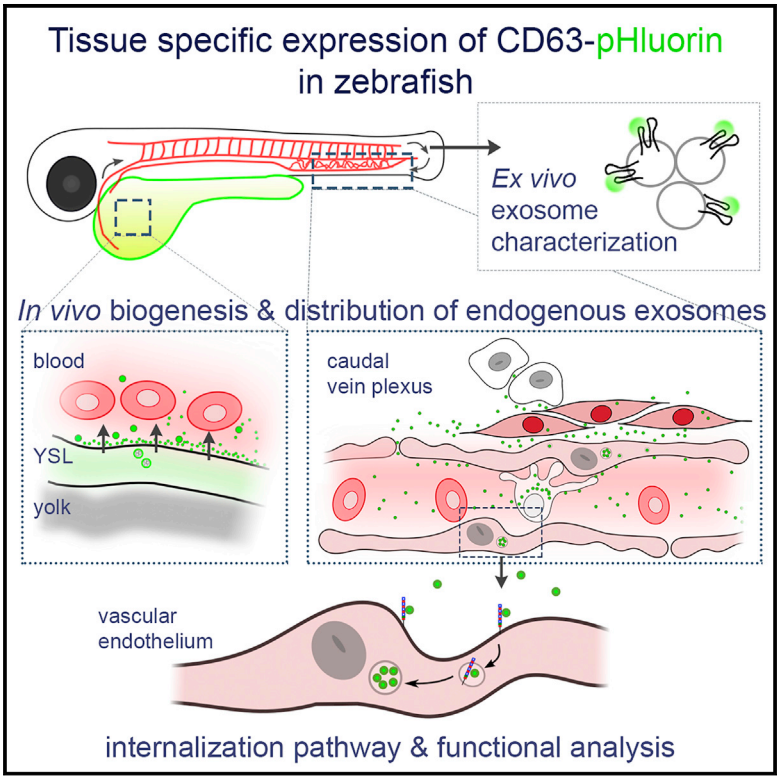

Highlights

- Single endogenous EVs can be live-visualized in the zebrafish embryo with CD63-pHluorin
- Syntenin in the YSL regulates exosome release into the blood for further dissemination
- YSL exosomes are taken up by macrophages and endothelial cells in the tail of the embryo
- Uptake is scavenger receptor- and dynamin-dependent and provides trophic support

Authors

Frederik J. Verweij, Celine Revenu, Guillaume Arras, ..., Filippo Del Bene, Graça Raposo, Guillaume van Niel

Correspondence

frederik.verweij@inserm.fr (F.J.V.), guillaume.van-niel@inserm.fr (G.v.N.)

In Brief

Verweij et al. develop an *in vivo* model using zebrafish embryos to live-track the production, journey, and fate of individual exosomes. Using a combination of imaging methods and proteomic analysis, they investigate the composition of endogenous exosomes and the molecular mechanisms controlling their biogenesis, fates, and functions in receiving cells.

Verweij et al., 2019, Developmental Cell *48*, 573–589
February 25, 2019
https://doi.org/10.1016/j.devcel.2019.01.004

CellPress

Developmental Cell
Resource

Live Tracking of Inter-organ Communication by Endogenous Exosomes *In Vivo*

Frederik J. Verweij,[1,2,*] Celine Revenu,[3] Guillaume Arras,[4] Florent Dingli,[4] Damarys Loew,[4] D. Michiel Pegtel,[5] Gautier Follain,[6] Guillaume Allio,[6] Jacky G. Goetz,[6] Pascale Zimmermann,[7] Philippe Herbomel,[8] Filippo Del Bene,[3] Graça Raposo,[1] and Guillaume van Niel[1,2,9,*]

[1]Institut Curie, PSL Research University, CNRS UMR144, Paris 75005, France
[2]Institute for Psychiatry and Neuroscience Paris, Hopital Saint-Anne, Université Descartes, INSERM U894, Paris 75014, France
[3]Institut Curie, PSL Research University, INSERM U934, CNRS UMR3215, Sorbonne Université, Paris 75005, France
[4]Institut Curie, PSL Research University, Centre de Recherche, Laboratoire de Spectrométrie de Masse Protéomique, Paris, France
[5]Department of Pathology, Cancer Center Amsterdam, the Netherlands
[6]INSERM UMR_S1109, Université de Strasbourg, Fédération de Médecine Translationnelle de Strasbourg, Strasbourg, France
[7]Centre de Recherche en Cancérologie de Marseille, Aix-Marseille Université, Marseille 13284, France
[8]Institut Pasteur, Department of Developmental & Stem Cell Biology, 25 rue du Dr Roux, Paris 75015, France
[9]Lead Contact
*Correspondence: frederik.verweij@inserm.fr (F.J.V.), guillaume.van-niel@inserm.fr (G.v.N.)
https://doi.org/10.1016/j.devcel.2019.01.004

SUMMARY

Extracellular vesicles (EVs) are released by most cell types but providing evidence for their physiological relevance remains challenging due to a lack of appropriate model organisms. Here, we developed an *in vivo* model to study EV function by expressing CD63-pHluorin in zebrafish embryos. A combination of imaging methods and proteomic analysis allowed us to study biogenesis, composition, transfer, uptake, and fate of individual endogenous EVs. We identified a subpopulation of EVs with exosome features, released in a syntenin-dependent manner from the yolk syncytial layer into the blood circulation. These exosomes are captured, endocytosed, and degraded by patrolling macrophages and endothelial cells in the caudal vein plexus (CVP) in a scavenger receptor- and dynamin-dependent manner. Interference with exosome biogenesis affected CVP growth, suggesting a role in trophic support. Altogether, our work represents a system for studying endogenous EV function *in vivo* with high spatiotemporal accuracy, demonstrating functional inter-organ communication by exosomes.

INTRODUCTION

Extracellular vesicles (EVs) collectively include exosomes, 50–200 nm diameter membranous vesicles secreted from multivesicular endosomes (MVEs) fusing with the plasma membrane (PM), and microvesicles (MVs), 50–1 μm diameter membranous vesicles that bud from the PM. Exosomes and MVs are released by a wide variety of cell types and are found in all organisms investigated so far (van Niel et al., 2018). Their implication in an increasing number of major physiological and pathological processes supports their putative role as essential intercellular messengers (Lo Cicero et al., 2015; Tkach and Théry, 2016). Most of the data on the function of EVs such as exosomes, however, are gathered from transformed cancer cells and rely on the use of a heterogeneous population of EVs purified from cell culture supernatant or liquid biopsies. Consequently, the propagation of endogenous exosomes *in vivo* is largely unknown, and data on their biogenesis and role in normal developing tissue and adult tissue homeostasis distinctly lag behind. Understanding EV biogenesis, transfer, and fate in recipient cells, however, is of prime importance not only from a fundamental point of view but also to assess their relevance in pathological conditions as well as their use as therapeutic delivery systems (Fais et al., 2016). This apparent hiatus is largely due to the shortage of suitable models to visualize and track single endogenous EVs and in particular exosomes *in vivo* from their site of production to their final destination in target cells (Hyenne and Goetz, 2017). Previous studies visualizing EV release and transfer have been limited to the detection of larger extracellular structures or their transfer from transplanted transformed cells (Lai et al., 2015; Zomer et al., 2015).

Our main aim was to develop an integrated model to study EV release, transfer, and function, which combines *in vivo* imaging with sub-cellular resolution while retaining the *in toto* imaging scale. Due to their small size and transparency, zebrafish embryos elegantly match the single-cell precision of *C. elegans* research in a vertebrate system with relevant architectural homology with mice and human. We show here that zebrafish embryos can be used to track exosomes *in vivo* by expression of the CD63-pHluorin reporter. This fluorescent reporter is specifically targeted to (late-) endosomes and secreted on exosomes, allowing live visualization of exosome release in single cells *in vitro* (Verweij et al., 2018). Expression of CD63-pHluorin in zebrafish embryos revealed massive release of exosomes from the yolk syncytial layer (YSL) into the blood flow that could be tracked *in vivo* throughout the animal up to their final destination. These exosomes are arrested and taken up by macrophages and endothelial cells of the caudal vein plexus (CVP) in a dynamin-dependent manner for degradation in lysosomes. Interference with syntenin-dependent exosome biogenesis in the YSL affected CVP growth, supporting a trophic role of these exosomes. Altogether,

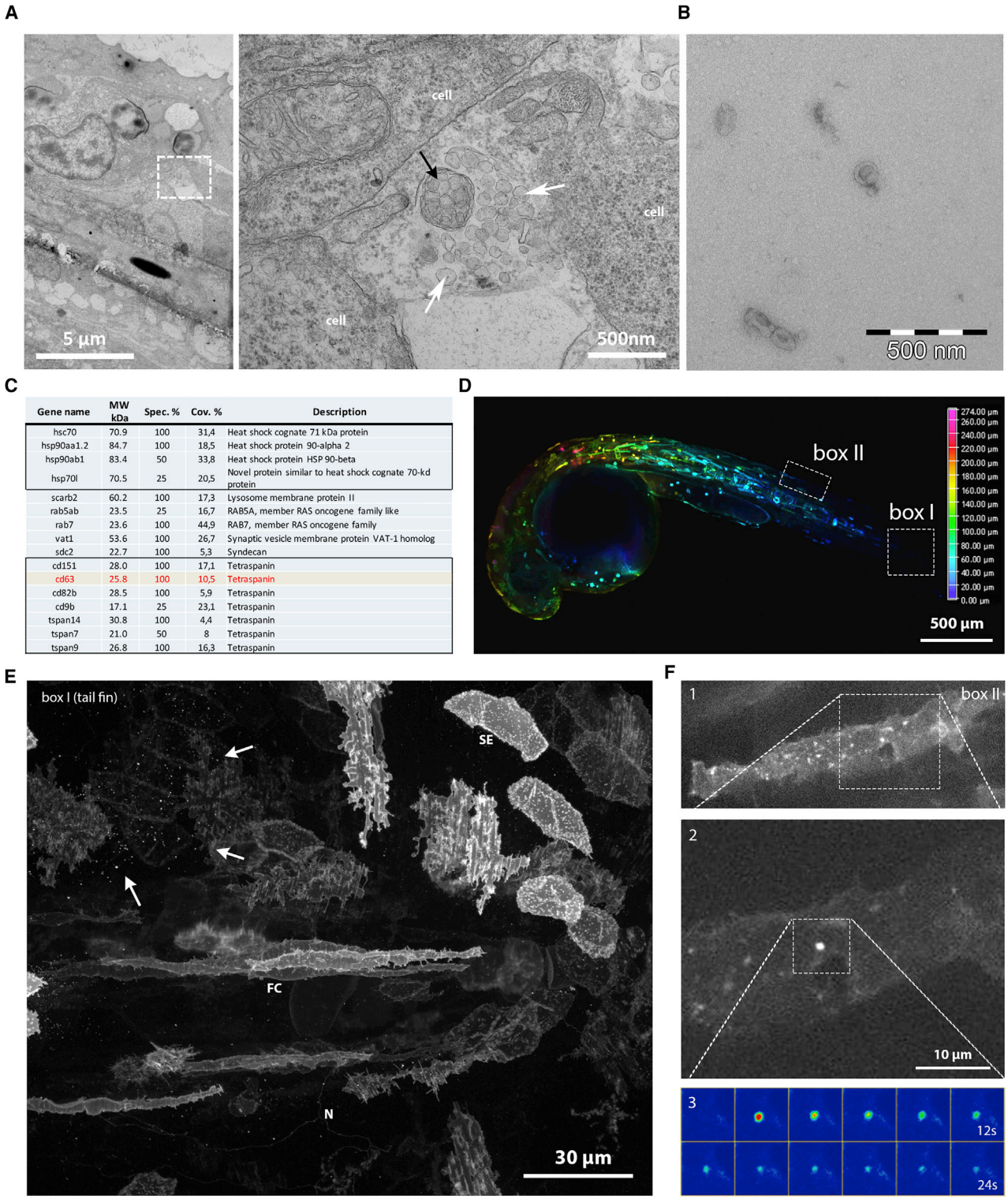

Gene name	MW kDa	Spec. %	Cov. %	Description
hsc70	70.9	100	31,4	Heat shock cognate 71 kDa protein
hsp90aa1.2	84.7	100	18,5	Heat shock protein 90-alpha 2
hsp90ab1	83.4	50	33,8	Heat shock protein HSP 90-beta
hsp70l	70.5	25	20,5	Novel protein similar to heat shock cognate 70-kd protein
scarb2	60.2	100	17,3	Lysosome membrane protein II
rab5ab	23.5	25	16,7	RAB5A, member RAS oncogene family like
rab7	23.6	100	44,9	RAB7, member RAS oncogene family
vat1	53.6	100	26,7	Synaptic vesicle membrane protein VAT-1 homolog
sdc2	22.7	100	5,3	Syndecan
cd151	28.0	100	17,1	Tetraspanin
cd63	25.8	100	10,5	Tetraspanin
cd82b	28.5	100	5,9	Tetraspanin
cd9b	17.1	25	23,1	Tetraspanin
tspan14	30.8	100	4,4	Tetraspanin
tspan7	21.0	50	8	Tetraspanin
tspan9	26.8	100	16,3	Tetraspanin

Figure 1. Identification and *In Vivo* Visualization of EVs in Zebrafish

(A) Electron microscopic analysis of a 3 dpf zebrafish embryo showing heterogeneous EVs between basal epidermal cells. White arrows indicate exosome-like vesicles, and black arrow indicates an enwrapped cluster of vesicles.

(B) Electron microscopy observation of EVs purified by ultra-centrifugation from the supernatant of AB.9 caudal fibroblast cells.

(C) Mass spectrometry analysis of AB.9-derived EVs (excerpt, complete list in Table S1).

(legend continued on next page)

these data reveal for the first time the secretion, journey, and uptake in target cells of individual endogenous exosomes secreted *in vivo* and key molecular mediators of these processes.

RESULTS

Zebrafish Cells Secrete EVs Containing Exosomal Proteins

To investigate whether zebrafish could serve as a relevant model to study exosomes, we first assessed the presence of EVs in zebrafish embryos 3 days post-fertilization (dpf) by electron microscopy (EM). EM analysis revealed the presence of 100 to 200 nm diameter vesicles clustered and enwrapped or free in the extracellular space (Figure 1A). We also processed the cell-culture supernatant of the zebrafish fibroblast AB.9 cell line with a differential ultra-centrifugation protocol (Théry et al., 2006). Using EM, we detected various vesicles in the size range of exosomes (~100 nm) (Figure 1B). Proteomic analysis on the same preparations identified a variety of zebrafish homolog proteins traditionally found in mammalian exosomes, including tetraspanins CD63, CD9, and CD82, and several heat shock proteins (HSPs), including HSP70 and HSP90 (Figure 1C; Table S1), and similar to the markers identified in exosomes derived from Zmel cells, a zebrafish melanoma cell line (Hyenne et al., 2019, this issue of *Developmental Cell*). This demonstrates that zebrafish cells release EVs that are enriched in the CD63 zebrafish ortholog, and supports the application in zebrafish of the fluorescent reporter hCD63-pHluorin, which we recently used to visualize the fusion of MVEs with the PM *in vitro*, (Verweij et al., 2018). Due to its pH-sensitivity, CD63-pHluorin primarily reports its "extracellular pool" (i.e., PM and EVs) but obscures CD63 large intracellular pool present in acidic endosomal compartments (Sung et al., 2015). Injection of ubi:hCD63-pHluorin plasmid-DNA (pDNA) at the single-cell stage of Casper zebrafish embryos resulted in mosaic, transient expression of CD63-pHluorin in multiple cell types, including epithelial, endothelial, neuronal, red blood cells, and muscle cells without obvious developmental defect of the embryo (Figures 1D and 1E). CD63-pHluorin-associated fluorescence was localized at the PM of these cell types and to small, dotty structures potentially corresponding to CD63-pHluorin-positive released EVs (Figure 1E, arrows). As previously shown in cell lines (Verweij et al., 2018), we could detect MVE-PM fusion events (Figure 1F, boxes 2 and 3) *in vivo*, which were pretty rare (~1 every 10 min) but with similar duration when compared to our observations in various cell lines *in vitro* (i.e., 20–30 s) (Verweij et al., 2018). Current technical limitations of imaging restricted the detection of MVE-PM fusion events *in vivo* to flat, stretched cells close to the dermis such as long-stretched fibroblast-like cell types (Figure 1F).

A Major Pool of CD63-Positive EVs Is Present in the Bloodstream of Zebrafish Embryos

One of the postulated assets of EVs is their potential as extracellular carriers in long-range communication *in vivo* by entering the circulation (Thomou et al., 2017; Tkach and Théry, 2016). Despite circumstantial evidence, this has never been studied directly in a relevant physiological *in vivo* model. In zebrafish embryos, the cardiovascular system develops with a heartbeat and a first transient wave of erythrocytes as early as at 24 h post-fertilization (Hermkens et al., 2015). Strikingly, in 3 dpf zebrafish larvae expressing CD63-pHluorin, we could detect a large pool of CD63-pHluorin-positive membranous structures carried by the blood flow in different parts of the vasculature throughout the body, including the brain and the gills (Figures 2A and 2B; Video S1). EM analysis on blood vessels of ubi:CD63-pHluorin plasmid (p)DNA-expressing embryos confirmed the presence of numerous single EVs in the size range of exosomes (~100 nm), but also a minor fraction of trapped vesicles and multivesicular structures that labeled positive for immunogold associated to anti-GFP antibody (Figures 2C–2E). While the initial observations were done on 3 dpf embryos, we could detect CD63-positive EVs as early as 24 h (1 dpf), at the onset of the blood flow (data not shown). This observation opened the opportunity to track individual endogenous EVs *in vivo*.

The Yolk Syncytial Layer Releases CD63-pHluorin-Positive Exosomes in the Bloodstream

Next, we aimed to identify the cellular origin of the CD63-positive EVs detected in the bloodstream. The large surface area of the YSL, its highly differentiated secretory apparatus, high lysosomal activity, and cytoplasmic multivesicular structures by EM (Walzer and Schönenberger, 1979) made a plausible candidate for the vast number of EVs detected in the blood flow. Moreover, until the duct of Cuvier closes at day 2.5, then forming the common cardinal vein (CV), the YSL is in direct contact with the blood flow (Helker et al., 2013). Video-enhanced Nomarski microscopy revealed numerous EVs in the large interstitial space between the YSL and the overlying epidermis, at and even before the onset of blood circulation (Figure S1A). Injection of ubi:CD63-pHluorin pDNA directly in the YSL at the 1,000-cell stage (4 hpf) (Figure S1B) allowed for tissue-specific expression of CD63-pHluorin and circumvented the need for tissue-specific promoters (Figure 3A). Immunogold labeling for GFP on thin cryosections of YSL CD63-pHluorin expressing 3 dpf zebrafish embryos showed a massive number of vesicles ranging from 80 to 200 nm in size immediately above the YSL and in direct contact with the blood (Figures 3B–3C and S1C). Consistently, CD63-pHluorin-positive EVs were detected in the blood flow after tissue-specific expression of CD63-pHluorin in the YSL (Video S2), and EM analysis of the blood vessels confirmed the nature of the fluorescent structures as single vesicles enriched in CD63-pHluorin in the size range of exosomes (~100–150 nm) (Figure 3D). Moreover, YSL-derived EVs that were observed in the blood flow accumulated in the CVP only in embryos with a detectable bloodstream (Figure 3E). This indicates that YSL-derived EVs enriched in CD63-pHluorin are continuously released in the blood flow and can circulate through the entire embryo to reach their remote destination.

(D) Transient mosaic expression of ubi:CD63-pHluorin in 35 hpf zebrafish embryo, pseudo-colored for depth.
(E) Example of cell types in caudal fin targeted by transient mosaic expression of CD63-pHluorin (3 dpf). Identified as, among others, skin epithelial (SE), neuronal (N), and fibroblast cells (FC). Arrows point at labeled EV.
(F) Example of a fusion event observed in a fibroblast-like cell (1), with zoom in (2), and time-lapse heatmap of the event (3).

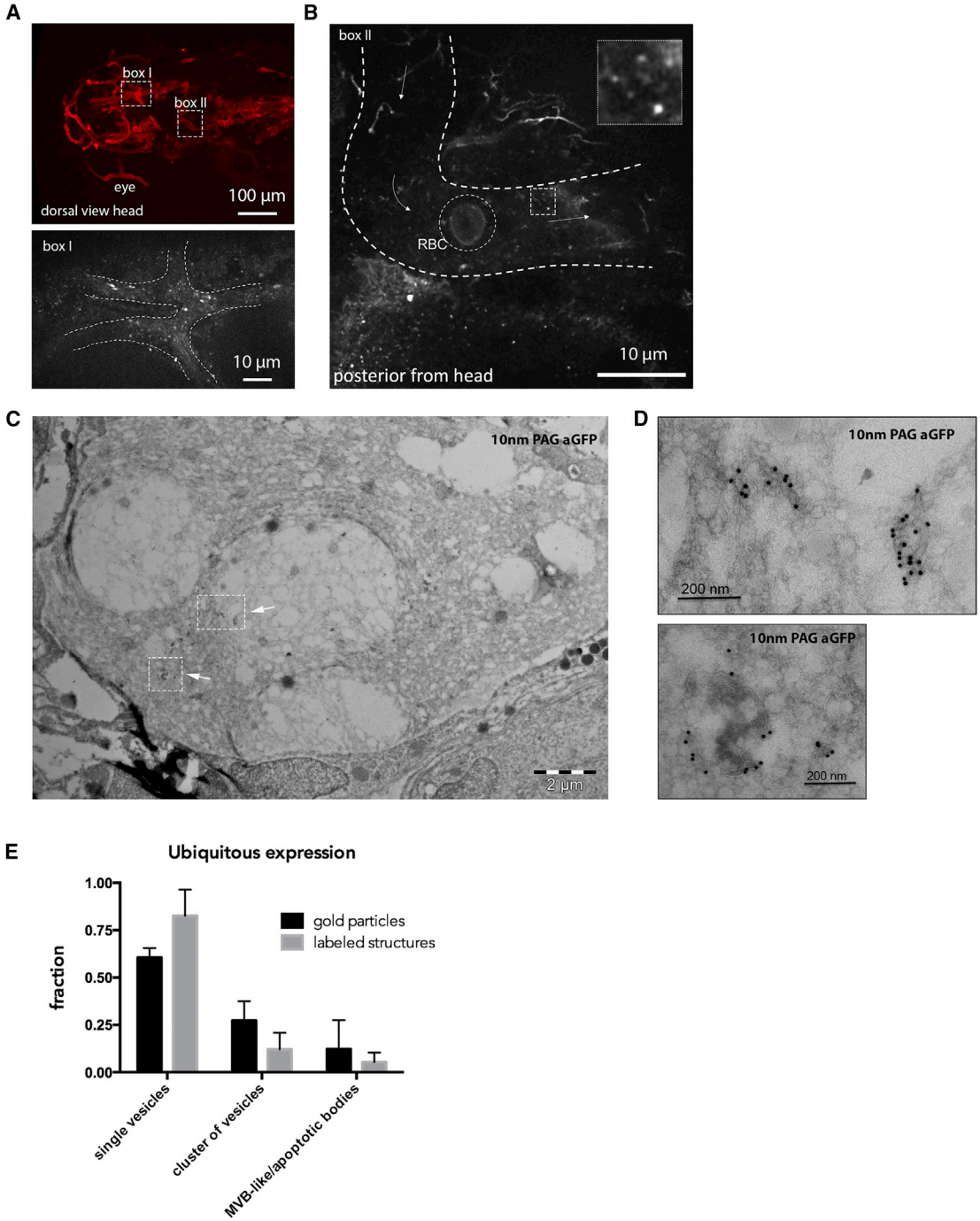

Figure 2. EVs Travel through the Blood Flow

(A) Dorsal view of the vasculature in the head of a *Tg(kdrl:Hsa.HRAS-mCherry)* 3 dpf zebrafish larva expressing CD63-pHluorin after injection of ubi:CD63-pHluorin pDNA at the 1-cell stage. Boxes I and II indicate areas of interest imaged for CD63-pHluorin, shown in (A) (lower panel) and (B).

(B) Still of time-lapse sequence shown in Video S1A, indicating the approximate vasculature wall (dashed white lines), a red blood cell (RBC), and in the dotted box, a sample of EVs seen in the bloodstream, which is magnified in the insert. Arrows indicate the direction of the blood flow.

(C and D) IEM on the vasculature of ubi:CD63-pHluorin pDNA-injected fish (transient mosaic expression), labeled with gold particles directed to GFP (10 nm), showing (D) single vesicle (upper panel) and clusters (lower panel) of vesicles, corresponding to the dotted boxes in (C).

(E) Quantification of vesicle labeling and appearance (single/clustered) of EVs as in (C) (mean ± SD, >25 different fields, n = 2).

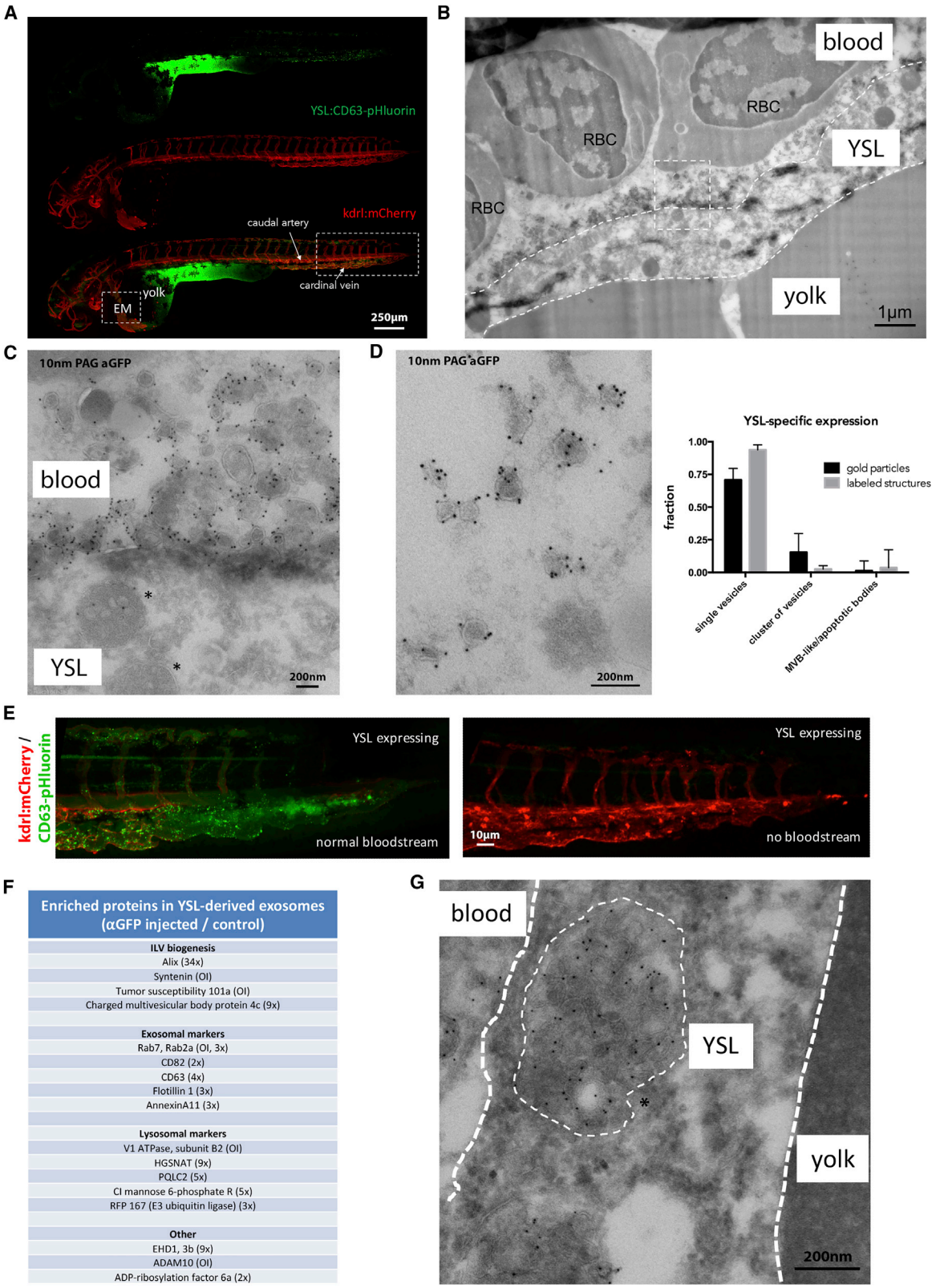

Enriched proteins in YSL-derived exosomes (αGFP injected / control)
ILV biogenesis
Alix (34x)
Syntenin (OI)
Tumor susceptibility 101a (OI)
Charged multivesicular body protein 4c (9x)
Exosomal markers
Rab7, Rab2a (OI, 3x)
CD82 (2x)
CD63 (4x)
Flotillin 1 (3x)
AnnexinA11 (3x)
Lysosomal markers
V1 ATPase, subunit B2 (OI)
HGSNAT (9x)
PQLC2 (5x)
CI mannose 6-phosphate R (5x)
RFP 167 (E3 ubiquitin ligase) (3x)
Other
EHD1, 3b (9x)
ADAM10 (OI)
ADP-ribosylation factor 6a (2x)

Figure 3. Origin and Composition of Exosomes in the Blood Flow

(A, B, D, and E) Fluorescence image of a 3 dpf *Tg(kdrl:Hsa.HRAS-mCherry)* embryo injected with ubi:CD63-pHluorin in the YSL, green channel (top), red channel (middle), and merge (bottom). Box [EM] indicates the approximate region for EM analysis, shown in (B) and (D). Box to the right indicates the area shown in (E).

(legend continued on next page)

Next, we characterized the nature of these fluorescent EVs by dissociating 3 dpf CD63-pHluorin YSL-expressing and YSL-non-expressing control embryos using Collagenase I treatment and isolating EVs from the supernatant with a differential ultra-centrifugation protocol (Théry et al., 2006). Immunogold labeling followed by EM observation of the CD63-pHluorin YSL-expressing-embryos-derived pellet (Figure S1C) confirmed the presence of vesicles heavily labeled for CD63-pHluorin with a morphology and a size (80–120 nm) comparable to those observed by EM *in situ* (Figure 3D). Whereas larger EVs were visible in the pellets, less than 5% of the labeled vesicles was larger than 150 nm in size (Figures S1C and S1D). Nanoparticle tracking analysis (Figure S1E) of the 100,000 g pellet of both conditions did not show significant differences in terms of size and number, suggesting that the expression of CD63-pHluorin in the YSL did not profoundly affect the release of EVs compared to basal condition. Pellets from both conditions were then further processed by immunoprecipitation against GFP using GFP-Trap agarose beads, followed by quantitative label-free proteomic analysis of the pull-down fraction. We quantified enrichment of specific proteins using non-injected zebrafish-derived EV pellet as background. The most enriched proteins were syntenin-a, TSG101, Rab7, ADAM10, and V1 ATPase subunit B2, which were only detected in the injected YSL EV-fraction and Alix (34×). Other YSL EV-enriched proteins included CMHP4c, EHD1, Cation-Independent Mannose 6-phosphate Receptor, Flotillin 1, CD63, CD82, the lysosomal acetyltransferase HGSNAT, and the lysosomal amino acid transporter PQLC2. (Figure 3F; Table S2). Of note, several of the enriched proteins are implicated in one of the machineries involved in exosome biogenesis in endosomes *in vitro* (Baietti et al., 2012). These data strongly support an endosomal origin of YSL-derived EVs. This conclusion was reinforced by the presence of large MVEs that contain CD63-pHluorin-positive intraluminal vesicles (ILVs) (Figure 3G) in the YSL. Thus, CD63-pHluorin-positive YSL-EVs present all the characteristics of endosome-derived exosomes as previously defined (Gould and Raposo, 2013). Finally, these YSL-exosomes were enriched for Molecular function Gene Oncology (GO) terms "Anion binding," "Small molecule binding," and "Transporter activity," with the latter being characterized by the presence of several solute carrier family proteins, including zinc and amino acid transporters slc30a1a and slc3a2b. YSL-derived exosomes displayed similarities with the composition of the AB.9 caudal fibroblast-derived exosomes and to a certain extent with Zmel zebrafish cell line-derived EVs (Table S1; Hyenne et al., 2019), as they both contain major actors of exosome biogenesis (Alix, TSG101, Chmp4C, and tetraspanins). Nevertheless, physiological (this study) and pathological (Hyenne et al., 2019) exosomes differed by their composition that could be linked to their respective (patho)physiology (Table S2). Altogether, these data strongly suggest that expression of CD63-pHluorin in the YSL reveals the release of exosomes in the bloodstream of developing embryos.

YSL-Derived CD63-Positive Exosomes Adhere to Endothelial Cells of the Caudal Plexus and Are Actively Endocytosed by Patrolling Macrophages

Having determined a cell layer of origin and transportation route of CD63-positive exosomes, we live-tracked them in the blood vasculature to identify potential target cells. Our data revealed an accumulation of dotty signals (Figure 3A) likely corresponding to immobilized exosomes in the blood, in particular in the caudal part of the vasculature. This area comprises the caudal artery (CA) and a complex, venous vascular network in between and originating from the CV, called the CVP (Figure 4A).

A maximum projection time-lapse movie of this region at higher magnification suggested an interaction between the labeled exosomes and the vessel wall (Figure 4A; Video S3A). Indeed, high-speed imaging of the CV confirmed the transient interaction of exosomes passing through the blood vessels with the PM of endothelial cells (Figure 4B; Video S3B). To visualize the extent and the exact localization of exosomes that adhere in the caudal part of the vasculature, we created a heatmap overlay of 6 individual YSL CD63-pHluorin pDNA-injected embryos at 3 dpf (Figure 4C). Strikingly, the vast majority of exosomes were selectively arrested in the venous plexus and the caudal vein but not in the CA. This behavior is remarkably similar to what was observed for intravenously injected Zmel1 EVs (Hyenne et al., 2019), suggesting a common behavior for EVs of distinct origin and labeled with different tags in the blood flow of zebrafish embryos. In high-magnification images, we identified motile cells that crawled on the surface of the endothelial vessels and that contained labeled exosomes in intracellular compartments, likely resulting from their endocytosis (Figure 4D). Apart from endothelial cells, the lumen of the CVP hosts a number of embryonic macrophages that continuously scavenge their environment and stand out by their relative high motility (Murayama et al., 2006). In *Tg(kdrl:HRAS-mCherry)* zebrafish embryos, these macrophages can be distinguished by their mCherry-positive compartments, probably as a result of endocytosis of (apoptotic) fragments of mCherry-expressing endothelial cells. By exploiting a *Tg(mpeg1:mCherryF)* fish line that specifically labels macrophages in red, we could identify these exosome-internalizing cells as patrolling macrophages (Figure 4E; Video S4A). Subsequent time-lapse imaging of macrophages in the caudal plexus of *Tg(kdrl:HRAS-mCherry)* fish expressing CD63-pHluorin in the YSL revealed an active form of

(B) IEM image of the YSL of a 3 dpf *Tg(kdrl:Hsa.HRAS-mCherry)* embryo injected with ubi:CD63-pHluorin in the YSL labeled with gold particles directed to GFP (10 nm). Dashed white lines indicate the approximate membranes of the YSL. Dashed line box indicates area shown enlarged in (C). RBC, red blood cell.
(C) Zoom in of area indicated in (B), showing MVE (asterisk) in the YSL, and EVs labeled for gold particles directed to GFP (10 nm) on top of the YSL.
(D) (Left panel) IEM image of exosome-sized EVs observed in blood vessel lumen, labeled with gold particles directed to GFP (10 nm). Graph on the right: quantification of vesicle labeling and appearance as in Figure 2E (mean ± SD, >25 different fields, n = 2).
(E) Zoom in on area indicated with rectangular box on the right in (A). (Left panel) Fish with blood flow; (Right panel) fish without blood flow, both expressing CD63-pHluorin in the YSL.
(F) Mass-spectrometry analysis of enriched proteins in YSL-derived EVs (excerpt, complete list in Table S2) (numbers between bracket indicated the rate of enrichment in injected embryos compared to control embryos; OI, only detected in injected embryos).
(G) IEM image of an MVE in the YSL area, labeled with gold particles directed to GFP (10 nm). Thin dashed white circle indicates an MVE. YSL, yolk syncytial layer; MVE, multivesicular endosome.

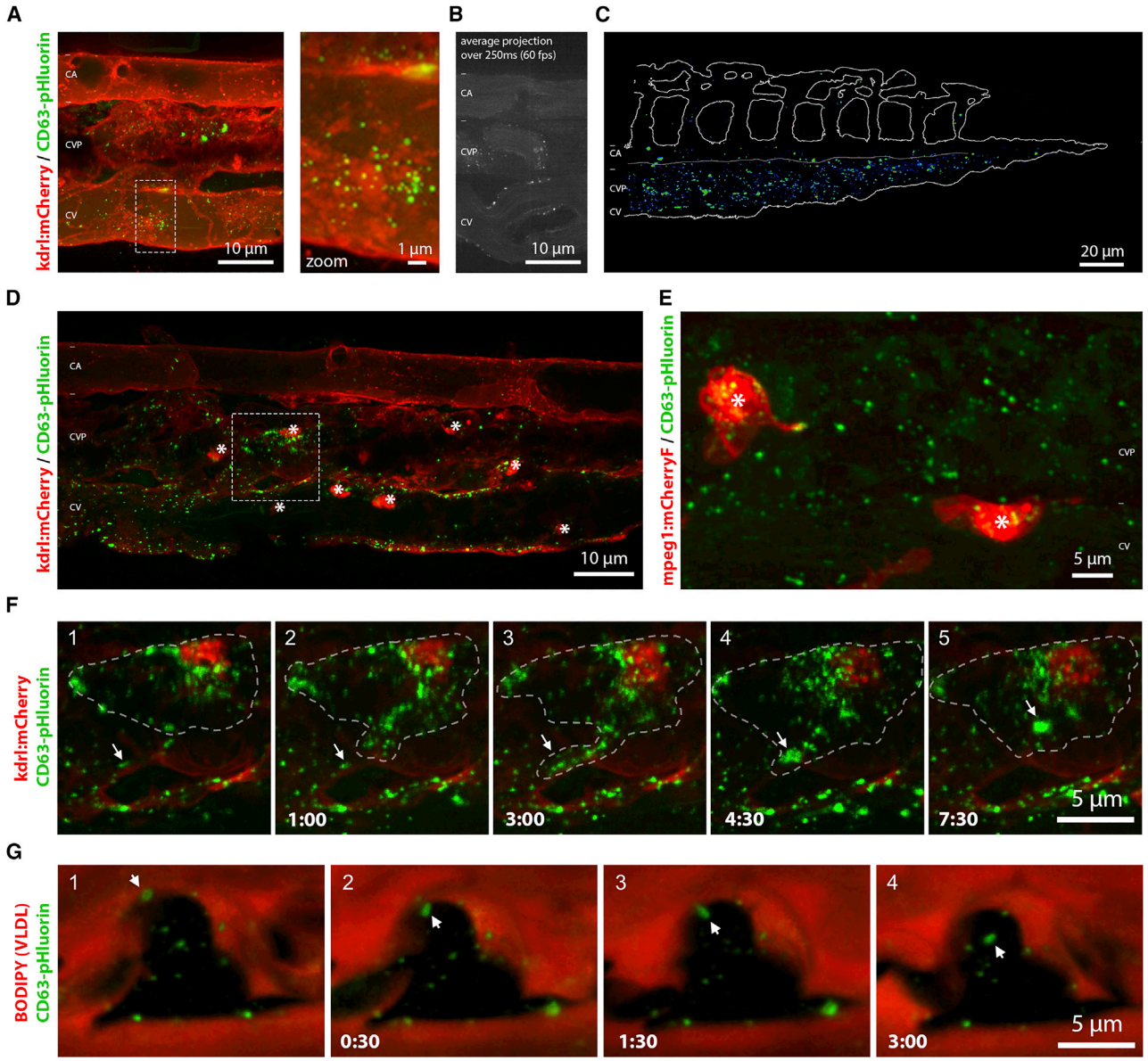

Figure 4. Distribution and Target Cells of YSL Exosomes

(A) Still of time-lapse shown in Video S3A of the CVP of a 3 dpf *Tg(kdrl:Hsa.HRAS-mCherry)* embryo expressing CD63-pHluorin in the YSL. Dashed box indicates area shown at higher magnification to the right.

(B) Average projection of 15 sequential frames of Video S3B, showing caudal artery (CA), CVP, and the cardinal vein (CV) in 3 dpf zebrafish embryos expressing CD63-pHluorin in the YSL.

(C) Heatmap of CD63-pHluorin signal in CVP of 6 3 dpf *Tg(kdrl:Hsa.HRAS-mCherry)* zebrafish embryos expressing CD63-pHluorin in the YSL.

(D) CVP of a 3 dpf *Tg(kdrl:Hsa.HRAS-mCherry)* embryo expressing CD63-pHluorin in the YSL. Stars indicate macrophages. Dashed box indicates area shown in Video S4B and (F). Asterisks indicate macrophages.

(E) Still of Video S4A, showing the CVP of a 3 dpf *Tg(mpeg1:mCherryF)* expressing CD63-pHluorin in the YSL. Asterisks indicate macrophages.

(F) Time-lapse of a macrophage in a 3 dpf *Tg(kdrl:Hsa.HRAS-mCherry)* zebrafish embryo expressing CD63-pHluorin in the YSL, shown in Video S4B.

(G) Time-lapse of macrophage in a BODIPY-C12 injected 3 dpf zebrafish embryo expressing CD63-pHluorin in the YSL, shown in Video S4C. CA, caudal artery; YSL, yolk syncytial layer; CVP, caudal vein plexus.

uptake of exosomes by macrophages that projected dendrites or pseudopodia, able to interact and "harvest" exosomes from the surface of endothelial cells (Figure 4F; Video S4B). Similar "harvesting" by patrolling macrophages was also observed for melanoma-derived exogenous EVs (Hyenne et al., 2019), suggesting common mechanisms for the uptake of EVs of distinct origin.

To further investigate the specificity of the uptake of labeled exosomes by macrophages of the CVP, we injected the yolk of CD63-pHluorin YSL expressing Casper embryos at 1 dpf with

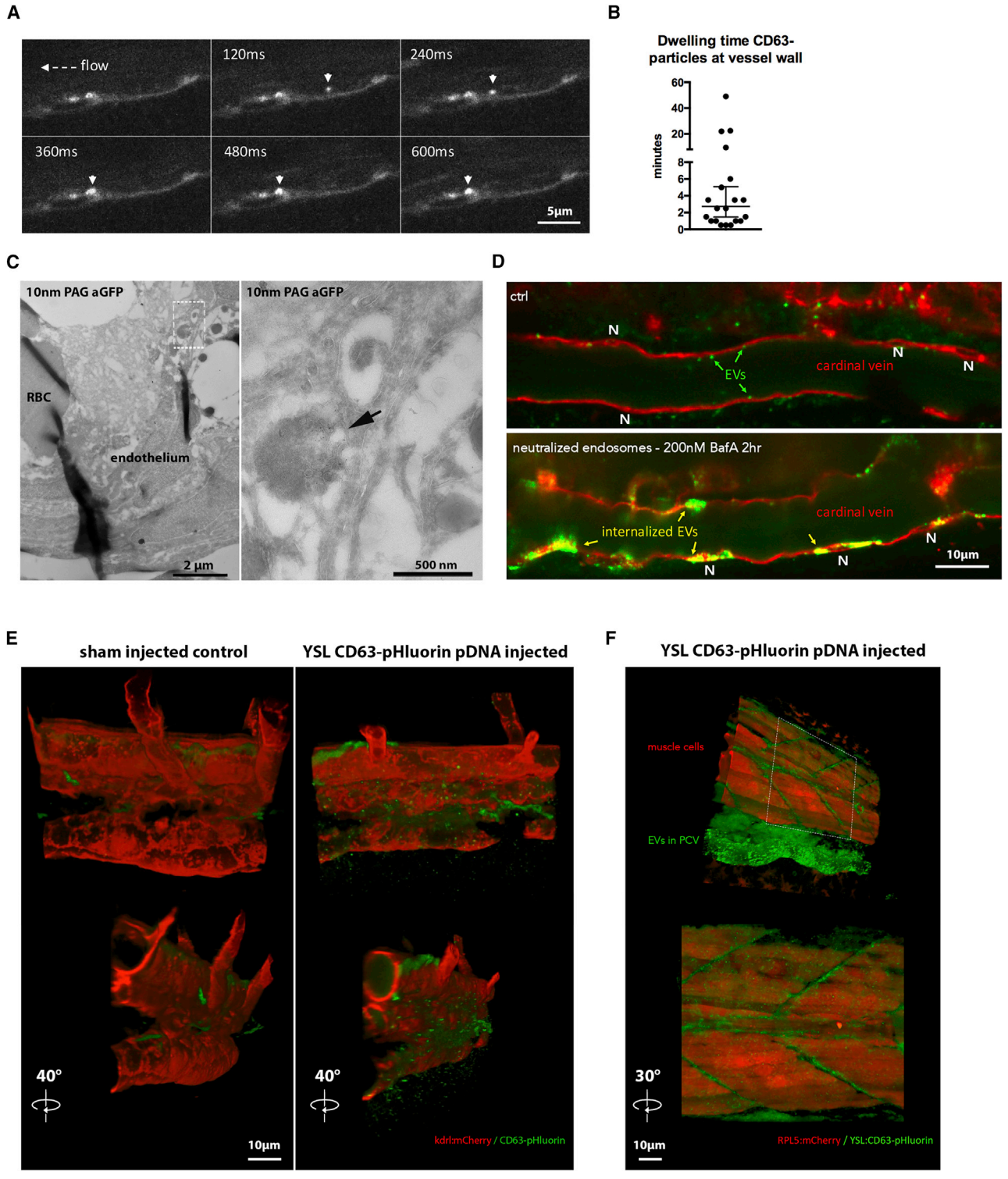

Figure 5. Interaction of YSL-Exosomes with Endothelium and Presence of YSL-Exosomes in ISF

(A) Time-lapse of Video S5A, showing the rolling and arrest of exosomes in the cardinal vein of 3 dpf zebrafish embryo expressing CD63-pHluorin in the YSL.

(B) Quantification of dwelling time of CD63-pHluorin exosomes at the vascular wall (mean ± SD, n = 20 events).

(C) EM image of the CVP of a 3 dpf zebrafish embryo expressing CD63-pHluorin in the YSL, labeled with gold particles directed to GFP (10 nm). Insert indicates area shown at higher magnification to the right. Arrow indicates internalized CD63-pHluorin exosomes in endo-lysosomal compartment of endothelial cell.

(legend continued on next page)

1.5 ng/nL BODIPY-C12 to specifically label the high amount of very-low-density lipoprotein (VLDL) particles produced by the YSL and released in the blood flow and to visualize the lumen of the blood vessels (Miyares et al., 2014). The BODIPY fluorescence was readily visible in the vasculature but was not overlapping with CD63-pHluorin labeling in the blood flow, confirming the nature of CD63-pHluorin-positive EV as exosomes and not as derivatives of VLDL. Moreover, we did not observe any BODIPY signal in macrophages, while exosomes were again actively endocytosed (Figure 4G; Video S4C). We did not observe an early decrease in fluorescence signal of CD63-pHluorin early (~3 min) after uptake (Figure 4G), in line with the observation of a large number of exosomes in the lumen of macrophages (Figures 4E and 4F), suggesting temporal "storage" and/or a delayed targeting to acidic endosomal compartments. Altogether, these data revealed a specific uptake of exosomes by macrophages in intracellular compartments that become acidic at later time point and/or that initially maintain connection with the cellular exterior.

YSL-Exosomes Are Taken Up and Degraded by Endothelial Cells

The specific interaction of labeled exosomes with the venous (Video S3), but not the arterial vasculature (Figure 4C), suggested potential implication of different shear forces exerted on EVs (Hyenne et al., 2019) between the venous and arterial blood flows. Drug treatment decreasing pacemaker activity (Vermot et al., 2009), and consequently the shear-force of the blood flow, did not lead to a visible increase of the association of exosomes with the CA (Figure S1F). This indicates the implication of additional factors, such as expression of adhesion molecules, in this interaction.

We further analyzed the dynamic of interaction between exosomes and the endothelium by using high-speed imaging of the caudal vein of YSL CD63-pHluorin pDNA-injected embryos 3 dpf. We observed rolling, arrest, and accumulation of exosomes on the endothelial wall of the vein (Figure 5A; Video S5A). Quantification of the duration of the interaction between exosomes and the venous vessel wall indicated that exosomes stay attached for an average duration of 3 min (Figure 5B). This behavior is similar to that of exogenous melanoma-derived EVs (Hyenne et al., 2019) and reinforced potential molecular interactions between exosomes and specific receptors at the surface of venous endothelial cells.

We observed that exosomes interacted transiently with endothelial cells and then disappeared (Figure 5B; Videos S3 and S5A), suggesting either their uptake by endothelial cells and targeting to acidic endosomal compartments, their re-entry into the blood flow, or dispersion outside of the vasculature. EM analysis of YSL CD63-pHluorin pDNA-injected zebrafish revealed, qualitatively, that the former occurs as we observed clusters of YSL derived exosomes immunogold labeled for GFP and mixed with dense aggregates in endo-lysosomal structures in endothelial cells of the caudal plexus (Figure 5C). This suggested a degradative fate of exosomes that we further investigated by treating zebrafish embryos with a specific inhibitor of the vacuolar H(+)-ATPase, Bafilomycin A1 (BafA), which elevates endosomal pH and decreases lysosomal degradation (Christensen et al., 2002). Strikingly, incubation for 2 h with 100 nm BafA showed that, consistent with sites of exosome-endothelium interaction (Figure 4C), endothelial cells of the vein plexus and CV but not the CA endocytosed considerable amounts of CD63-pHluorin exosomes over time, mostly concentrating at peri-nuclear areas (Figure 5D, nuclei indicated with (N)). This accumulation, after only two h of treatment, suggests that exosomes are mainly and continuously taken up by endothelial cells to be degraded in acidic endo-lysosomes.

We then tested whether exosomes could propagate beyond vascular endothelial walls. For this, we imaged the area of the CVP and clearly observed labeled exosomes outside of the posterior cardinal vein (PCV) (Figures 5E and 5F; Video S5B). Even though we observed some of the larger fluorescent exosome clusters concentrated adjacent to the CVP, we detected high levels of fluorescent exosomes outside of the vasculature throughout the whole embryo, notably visible where covering the muscle segments and flowing in the neural tube (Videos S5B and S5C). The motility of the exosomes we observed outside the vasculature was irregular and resembled Brownian motion, clearly distinct from the dynamics of intracellular endosomal transport (Video S5B). However, in muscle cells, Bafilomycin A treatment (Video S5D) did not show accumulation of YSL derived exosomes as observed for endothelial cells. The large majority of endocytosed exosomes was thus observed in endothelial cells and to a lesser extent in patrolling macrophages but not in other cell types, highlighting the specificity for targeted cells.

Uptake of YSL-Derived Exosomes by Endothelial Cells Relies on Scavenger Receptors and Dynamin-Dependent Endocytosis

This specific interaction of exosomes with target cell types likely relied on specific receptors (van Niel et al., 2018). The visualization of internalized CD63-pHluorin exosomes with BafA treatment, allowed us to interfere with general uptake mechanisms by inhibiting dynamin, a key regulator of clathrin dependent and independent endocytosis (Ferguson and De Camilli, 2012). We treated 2 dpf YSL CD63-pHluorin expressing *Tg(kdrl:HRAS-mCherry)* embryos, expressing mCherry in the vasculature, with 3 μM of dynamin inhibitor Pyrimidyn-7 prior to BafA treatment. Strikingly, we observed a near complete block of exosome uptake by endothelial cells (Figure 6A), excluding the uptake mechanisms of exosomes via dynamin independent pathways and possibly macropinocytosis (Harper et al., 2013). Mander's coefficient (M2) of the green signal (exosomes) overlapping with the red signal (endothelium) revealed an average decrease of more than 10-fold of the uptake (Figure 6B). Comparison of

(D) Close up of the cardinal vein of 3 dpf *Tg(kdrl:Hsa.HRAS-mCherry)* zebrafish embryos expressing CD63-pHluorin in the YSL, control-treated (DMSO), or treated with bafilomcinA (BafA) to neutralize acidic compartments.

(E) CVP area of 3 dpf *Tg(kdrl:Hsa.HRAS-mCherry)* zebrafish embryos sham-injected or injected with CD63-pHluorin pDNA in the YSL.

(F) Mid-trunk segment of 3 dpf zebrafish embryos expressing CD63-pHluorin in the YSL and mCherry under the ubiquitous RPL5 promoter. At this exposure level in the red channel, mostly muscle cells are visible. YSL, yolk syncytial layer; CVP, caudal vein plexus; PCV, posterior cardinal vein.

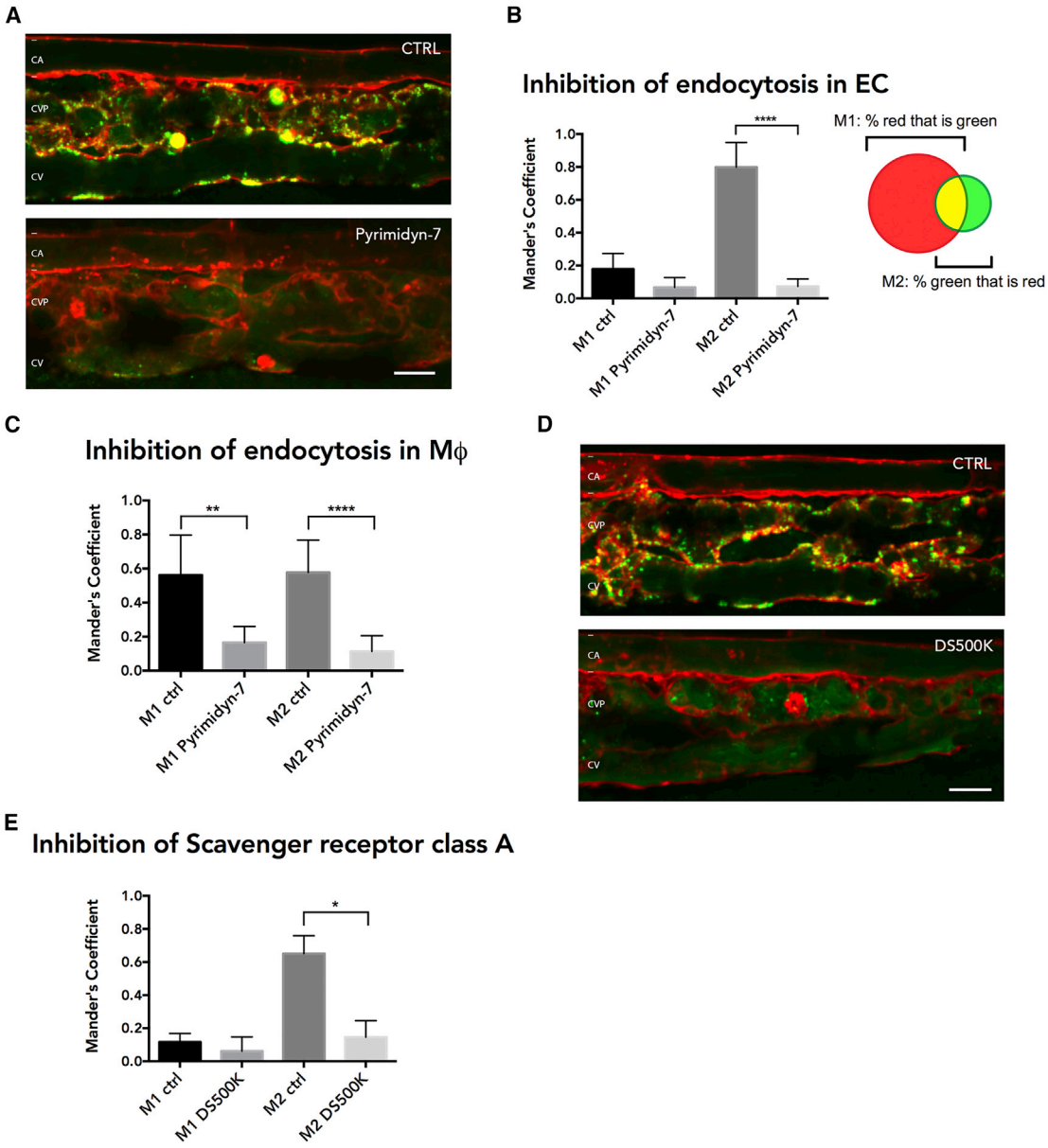

Figure 6. Characterization of Uptake Mechanism YSL-Exosomes by Endothelial Cells

(A) Close up of the CVP area of 3 dpf *Tg(kdrl:Hsa.HRAS-mCherry)* zebrafish embryos expressing CD63-pHluorin in the YSL, treated with BafA to show internalized EVs and co-treated with DMSO (CTRL) or dynamin-inhibitor Pyrimidyn-7 (Pyrimidin-7).

(B) Quantification of experiments as performed in (A), showing the overlap coefficient of red with green (M1) and green with red (M2) signal (mean ± SD, ****$p \leq 0.0001$; $n \geq 3$; unpaired t test with equal SD).

(C) As in (B), but for macrophages alone (mean ± SD, ****$p \leq 0.0001$; 7 macrophages per condition, $n \geq 3$; unpaired t test with equal SD).

(D) Close up of the CVP area of 3 dpf *Tg(kdrl:Hsa.HRAS-mCherry)* zebrafish embryos expressing CD63-pHluorin in the YSL treated with BafA to show internalized exosomes and non-injected or injected with 500K Dextran Sulfate (DS500K).

(E) Quantification of experiments as performed in (D) (mean ± SD, *$p \leq 0.05$; $n \geq 2$; unpaired t test with equal SD). YSL, yolk syncytial layer; BafA, bafilomycin A; CVP, caudal vein plexus. Scale bars represent 10 μm.

Mander's coefficient after 180-degree rotation excluded potential interference of random overlap (Figure S1G). Similar quantification in ctrl or Pyrimidyn-7 condition showed a 5-fold reduction of uptake in macrophages (Figure 6C).

To assess the efficiency of exosome uptake, we performed 4D imaging of the CV of 3 dpf YSL CD63-pHluorin expressing *Tg(kdrl:HRAS-mCherry)* embryos treated with 100 nM BafA. Time-lapse imaging indicated that exosomes accumulated over the ~1 h time-coursed imaged (Video S6A), whereas a z-stack and a 3D rendering of the same z-stack showed a substantial presence of internalized exosomes per cell (Video S6B). Similar findings were obtained at 2 dpf (data not shown).

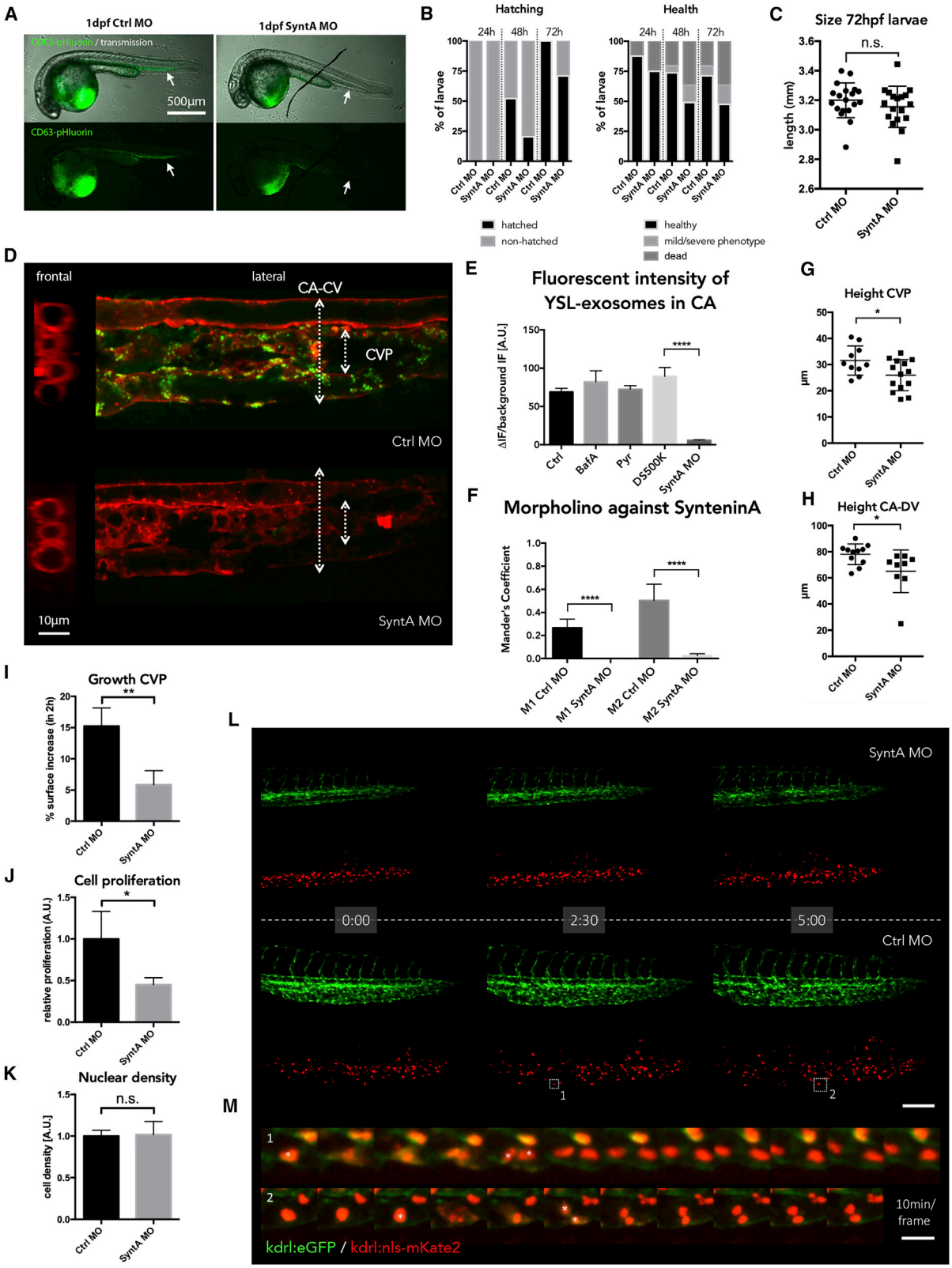

(legend on next page)

Together, this indicates that exosome uptake by the ECs of the CVP is not a sporadic event, but occurs in a continuous fashion. We next focused on potential receptors able to specify this endocytosis to endothelial cells.

Interestingly, the CVP area harbors scavenger endothelial cells (SECs) that interact in a scavenger-receptor mediated manner with liposomes of 100 nm injected in the circulation (Campbell et al., 2018). Scavenger receptors have also been reported *in vitro* to mediate exosome uptake (Plebanek et al., 2015); are expressed on endothelial cells and macrophages, and are conserved in teleost (Poynter et al., 2015); and mediate dynamin-dependent endocytosis (Jang et al., 2014). To investigate whether scavenger receptors are implicated in exosome uptake *in vivo*, we injected dextran sulfate ($DexSO_4$-500K), a known competitive ligand for scavenger receptors (Lysko et al., 1999), intravenously in CD63-pHluorin YSL expressing *Tg(kdrl:HRAS-mCherry)* embryos prior to BafA treatment. Strikingly, we observed a decrease of more than 4-fold of the green signal (EVs) overlapping with the red signal (endothelium) (Figures 6D and 6E), indicating that endogenous exosomes competed with $DexSO_4$-500K for their uptake by the same class of receptors. We did not observe a significant decrease in uptake in macrophages (Figure S1H).

This set of data revealed that *in vivo*, endogenous exosomes are specifically internalized by specialized venous endothelial cells in a dynamin- and scavenger receptor dependent pathway to be targeted to lysosomes for degradation.

Production of YSL-Derived Exosomes Relies on a Syntenin-Dependent Biogenesis Pathway and Supports Vasculogenesis of the Caudal Vein Plexus

The enrichment for a syntenin-ALIX mediated machinery in YSL-exosomes (Figure 3F) led us to interfere with their generation and further investigate their potential function *in vivo*. A previous study in zebrafish reported the expression of syntenin-a, notably in YSL, at different stages of development (Lambaerts et al., 2012). Depletion of syntenin-a in the whole embryo in the same study revealed defects in epiboly progression and body-axis formation during early zebrafish development, whereas depleting syntenin-a solely in the YSL only affected epiboly in 30% of the embryos and resulted in a well-formed axis in all embryos. We co-injected one of these morpholino (MO) oligonucleotides, validated in conformity to recently published guidelines (Stainier et al., 2017), targeting the translation start site in syntenin-a transcripts (SyntA MO) or control MO (Ctrl MO) together with CD63-pHluorin pDNA specifically in the YSL of *Tg(kdrl:HRAS-mCherry)* embryos 4 hpf. Of note, in our experiments most embryos displayed normal development but showed a small delay in hatching and increase in mortality (Figures 7A–7C). When considering only embryos with normal development (>50% in both conditions), whole body analysis showed expression of CD63-pHluorin in the YSL (Figure 7A) but a profoundly diminished number of fluorescent exosomes in the blood flow for the SyntA MO compared to the Ctrl MO condition (Figures 7D and 7E) that could be rescued by co-injection of MO-insensitive wt syntenin-a plasmid DNA (Figures S2A and S2B). This suggests that syntenin is implicated in CD63 positive exosome biogenesis in the YSL *in vivo* and that endogenous exosome biogenesis can be manipulated. Incubation of these embryos for 2 h with 100 nm BafA confirmed the near absence of exosomes in the CVP, corresponding with a 20-fold reduction of the uptake of exosomes by endothelial cells in this region (Figure 7F). While we did not observe any major defect in angiogenesis or growth of SyntA MO embryos at 3 dpf (Figure 7C), we did observe a decrease of ~18% in the height of the CVP between SyntA MO and Ctrl MO treated embryos (Figures 7G and 7H), suggesting a role of exosomes produced from the YSL in the development of the CVP by taking them up and targeting them to lysosomes. Finally, we aimed to further assess the effect of YSL-exosome depletion on CVP growth. For this, we performed imaging of YSL SyntA MO and Ctrl MO injected embryos over time between 35-40 hpf and quantified the number of nuclei and the expansion of the vascular bed (Figures 7I–7M). While the nuclear density was comparable, the growth of the CVP as well as the cell proliferation was lower in SyntA MO YSL-injected compared to Ctrl MO YSL-injected embryos (Figures 7I–7K), whereas cellular motility seemed unaffected. Together, this indicates that YSL exosomes support CVP growth, mainly by affecting cell proliferation.

Collectively, these data demonstrate that endogenous biogenesis of exosomes can be modulated, revealing physiological effects in defined target cells.

Figure 7. Functional Analysis of YSL-Exosomes

(A) Transmission and fluorescent images of Ctrl MO- or SyntA MO-treated 1 dpf zebrafish embryos.

(B) Quantification of morphological features of Ctrl MO- or SyntA MO-treated 1–3 dpf (24–72 h) zebrafish embryos. To the left, hatched versus non-hatched comparison. To the right, health status comparison with normal morphology (healthy), mild or severe developmental defects, and mortality. Sample size $\geq$ 120.

(C) Size (length) of Ctrl MO- or SyntA MO-treated 3 dpf zebrafish embryos (scatter-dot plot, mean ± SD; n = 19, n = 18, respectively).

(D) Close up of the CVP area of 3 dpf *Tg(kdrl:Hsa.HRAS-mCherry)* zebrafish embryos expressing CD63-pHluorin in the YSL, co-injected with Ctrl MO or SyntA MO in the YSL. Left panel: frontal view; right panel: lateral view. CA, caudal artery; CV, cardinal vein.

(E) Fluorescent intensity of GFP signal in CA measured during different treatments. BafA, bafilomycin-A; Pyr, Pyrimidyn-7; DS500K, 500 KDa dextran sulfate; SyntA MO, syntenin-a morpholino; A.U., arbitrary units. mean ± SD; ****p $\leq$ 0.0001; all conditions show at least triplicates of n $\geq$ 3; unpaired t test with equal SD.

(F) Quantification of overlap-coefficient of red with green (M1) and green with red (M2) in Ctrl MO- or SyntA MO-treated 3 dpf *Tg(kdrl:Hsa.HRAS-mCherry)* zebrafish embryos, as shown in (D) (mean ± SD; ****p $\leq$ 0.0001; n = 5; unpaired t test with equal SD).

(G and H) Quantification of height of caudal part of vasculature, specifically for the CVP at second intersegmental vessel (ISV), or (H) measured from CA to CV (scatter-dot plot, mean ± SD; *p $\leq$ 0.05; n $\geq$ 10, n $\geq$ 9 resp; unpaired t test with equal SD).

(I–K) *Tg(kdrl:eGFP /nls-mKate2)* embryos injected with control (Ctrl MO) or syntenin-a (SyntA MO) morpholinos in the YSL, analyzed for growth (I), proliferation (J), and nuclear density (K) in the CVP between 35 and 40 hpf (mean ± SD; *p $\leq$ 0.05; **p $\leq$ 0.01; n = 4; unpaired t test with equal SD).

(L) Time-lapse of *Tg(kdrl:eGFP /nls-mKate2)* embryos between 35 and 40 hpf. Boxes indicate 2 examples of proliferating cells. as shown in (M). Scale bar represents 40 μm.

(M) Two examples of dividing cells are shown. Scale bar represents 15 μm. YSL, yolk syncytial layer; CVP, caudal vein plexus.

DISCUSSION

Until now, the development of a model to explore the release, journey, and targets of endogenous exosomes *in vivo* had been hampered by the small size of the exosomes and the lack of appropriate methods to label them. A recent study reported the use of CD63-GFP in transgenic rats (Yoshimura et al., 2016) that demonstrated its usefulness for the *ex vivo* analysis of EV transfer to organs and bodily fluids but that was limited in its suitability for *in vivo* imaging. Here, we sought to fill that void by exploring a vertebrate model suitable for *in toto* imaging while maintaining sub-cellular and even supra-optical resolution. The CD63-pHluorin strategy has recently been shown to be an accurate *in vitro* model to explore new facets of the molecular mechanisms that control the biogenesis and secretion of exosomes (Verweij et al., 2018). Our study demonstrates that the CD63-pHluorin reporter can be used *in vivo* to investigate the molecular regulation of exosome secretion. However, this approach is currently still limited by a technological latch that hinders quantitative observation of bursts of fluorescence in cells that are not flat. In our model, we observed a relatively limited number of fusion events compared to transformed cell lines *in vitro*, which is in line with *in vitro* experiments indicating lower fusion activity for non-transformed cells (Verweij et al., 2018) as well as increased presence of exosomes in bodily fluids of cancer patients (Galindo-Hernandez et al., 2013; Logozzi et al., 2009). Interestingly, the transposition of this tool *in vivo* also provided a model allowing single vesicle tracking from their site of production to their final destination and might be useful to investigate the dynamics of body fluid flows with high precision (Bachy et al., 2008).

We observed a large number of fluorescent vesicles in the blood after ubiquitous expression of CD63-pHluorin. IEM labeling confirmed that CD63-pHluorin was associated to vesicular structures (Figures S1C and S2D). Using tissue-specific expression, we could trace the origin of these exosomes and identified the YSL, a secretory cell layer in direct contact with the blood, as one of the providers of endogenous exosomes that reach the rest of the organism. Mass spectrometry analysis of EVs derived from cell lines (AB.9, Zmel), embryos in our study, and in (Hyenne et al., 2019) showed a common composition and highlights a consistent presence of proteins involved in exosome biogenesis by the syntenin-Alix-ESCRT-III pathway, previously reported *in vitro* (Baietti et al., 2012). Our data strongly suggest that the EVs followed in this study are likely of endosomal origin, although we cannot exclude the contribution of the PM of the YSL as a source of EVs. Of note, treatment of embryos with GW4869 did not affect exosome release from the YSL (Figure S2E), suggesting that at least for this source of exosomes, ceramide is not a major regulator of their biogenesis (Trajkovic et al., 2008). These data suggest that *in vivo*, the syntenin-ALIX-ESCRT-III pathway is among one of the essential pathways for exosome biogenesis, opening avenues to interfere with EV generation and function *in vivo*.

Our initial explorations uncovered endothelial cells and patrolling macrophages as recipient cells, strengthening the notion of targeted communication by exosomes. Although we cannot exclude a specific role of YSL-derived exosomes once taken up by macrophages, these scavenger cells may harvest exosomes dwelling at the surface of endothelial cells to regulate the steady-state level of EVs in the circulation (Imai et al., 2015). However, we also observed that the internalizing compartments containing EVs (1) do not immediately acidify (Figure 4G) and (2) might be internalized slower, as we did not need to use bafilomycin A treatment to visualize uptake in macrophages and still observed green EVs in macrophages after prolonged incubation with DS500K (Figure S1H). This would be compatible with a functional interaction between the EVs and the macrophage, recently demonstrated in a cancer setting (Gabrusiewicz et al., 2018), and might be part of an immune surveillance function analogous to Kupffer cells (Jenne and Kubes, 2013). In zebrafish, we show that endogenous exosomes are mainly targeted to the venous endothelial cells of the CV(P). These cells show functional homology with specialized liver sinusoidal endothelial cells (LSECs) in higher vertebrates (Campbell et al., 2018), indicating inter-species correlation with the targeting of injected EVs to the liver in murine models (Charoenviriyakul et al., 2017; Wiklander et al., 2015). LSECs clear soluble macromolecules and small particles from the circulation and, in humans, possess the highest endocytic capacity of all cells (Poisson et al., 2017). In older vertebrates, jawless, cartilaginous, and bony fish, cells resembling the LSEC are located at different locations outside the liver and are collectively called SECs that are similarly central to the removal and catabolism of a variety of macromolecules from the circulation (Seternes et al., 2002).

We show that the uptake mechanisms of EVs by endothelial cells in the CV(P) implicate scavenger receptors and dynamin-dependent endocytosis. Indeed, various scavenger receptors internalize their ligands in a dynamin-dependent manner and traffic to lysosomes (Fukuda et al., 2011). Scavenger receptors, such as Stabilin-2, have been recently described as mediating the uptake of 100-nm-sized anionic liposomes in zebrafish (Campbell et al., 2018). This suggests that exosomes, having a negative z-potential (due to the presence of anionic lipids), could bind in a similar fashion to these receptors, independently of a specific ligand present on the exosomal membrane.

The lysosomal fate of YSL-derived exosomes in endothelial cells echoes data showing that uptake and catabolism of exosomes in lysosomal compartments is likely a major fate as described *in vitro* (Tian et al., 2010). This pathway would allow catabolism of EV content and provide a source of amino acids, nucleic acids, lipids, and ions to recipient cells. Although we cannot rule out a structural function of YSL-derived EVs during development, e.g., in patterning or differentiation (McGough and Vincent, 2016), the effect we observed on CV and CVP development when interfering with EVs biogenesis also suggests that endothelial cells may uptake and process EVs in lysosomes to use them as a source of macromolecules for their own development (Yao et al., 2017). It is also possible that these exosomes provide an extracellular source of membrane to allow for expansion of the vascular bed, analogous to the involvement of late endo/lysosomes in protrusions and neurite outgrowth (Naegeli et al., 2017; Raiborg et al., 2015). In accordance with this, we observed a lower proliferation rate of CVP endothelial cells with reduced levels of CD63 exosomes coming from the YSL (Figure 7J). These data raise the possibility that uptake of exosomes by LSEC, beyond a simple removal role of exosomes

from the circulation, indeed may support a trophic link between the YSL and LSCEs.

The presence of numerous EVs in the bloodstream but also in the interstitial fluid (ISF) of developing zebrafish embryos strengthens *ex vivo* observations of the presence of EVs in both fluids (Gromov et al., 2013; Johnstone et al., 1989). Recent evidence indicates that exosomes or EVs containing miRNAs can also in- and extravasate biological barriers to access ISF under physiological conditions (Thomou et al., 2017), but the YSL in zebrafish is directly connected with the ISF, providing a direct way for exosomes from YSL to access the ISF. The motility of the CD63-pHluorin-positive exosomes we observed outside the vasculature was irregular and resembled Brownian motion (Video S5B), clearly distinct from the dynamics of intracellular endosomal transport. Of note, bafilomycin A treatment (as in Figure 5D) did not show accumulation of YSL-derived exosomes in other cells such as the highly abundant muscle cells (Video S5D). These observations would exclude uptake and lysosomal degradation as a major way to use EVs as a source of macromolecules by other cells than endothelial cells. Of note, our proteomic analysis revealed the presence and enrichment for various lipid, amino acid, and ion transporters that could support a role of YSL-derived exosomes as "macromolecule dispenser" to the surrounding cells, as these transporters could potentially mediate the bioavailability of exosomal contents (Allen and Cullis, 2013). All in all, the presence of these EVs in various bodily fluids supports a general role in metabolism, e.g., in nutrient delivery, and makes a specific role in other YSL functions, e.g., embryonic patterning, less likely. Nevertheless, we cannot exclude that these EVs are used to exchange genetic information between cells *in vivo* as shown recently (Ashley et al., 2018; Pastuzyn et al., 2018; Zomer et al., 2015), and future development of adapted tools as described *in vitro* (Yim et al., 2016) is required to explore these functions in detail.

Despite its several advantages, we cannot exclude that in this model expression of this reporter might affect exosome secretion or composition. Nevertheless, nanoparticle tracking did not show a significant change in the number of particles between non-injected and CD63-pHluorin YSL-expressing embryos, and proteomics indicated the presence of endogenous zCD63 in the YSL-CD63-pHluorin labeled exosomes. Another potential downside of our approach might be that expression of a TSPAN-reporter may only label a subpopulation of YSL-derived exosomes as CD63 may not be equally enriched in all exosome subpopulation (Kowal et al., 2016). Larger (>150 nm) vesicles, predominantly negative for CD63-pHluorin, suggest the presence of different subpopulations in our model. Isolating a subpopulation from the heterogenous family of EVs with this reporter presents, however, the advantage to target specific fate or functions. Future studies using other TSPAN-pHluorin markers, including CD81, CD82, or CD9 (Verweij et al., 2018), could aid to cover the whole spectrum of EVs. The present study was restricted to the YSL, excluding from our observation all EVs released by other cell types that might represent up to 90% of the pelleted vesicles from dissociated fishes (Figures S1C and S2D). Development of future strains with cell-type-specific expression will allow investigation of the various roles of exosomes secreted under physiological and pathological conditions by nearly all cell types investigated so far. In addition, combining cell-type-specific expression of TSPAN-pHluorin markers with proteomic analysis of immuno-isolated exosomes could potentially be used to discover pathological biomarkers for each producing cell type targeted *in vivo*. What might also be considered as a drawback in some applications is that we use a pH-sensitive GFP, meaning that EVs that are taken up in recipient cells will in most cases likely end up in acidified compartments, resulting in quenching of their fluorescence. However, in this study, we do show that bafilomycin treatment reverts this acidification and consequently quenching of fluorescent EVs and the addition of a pH-insensitive fluorescent label to CD63-pHluorin can also be considered.

In this study, we opted for the MO strategy to achieve a tissue-specific knockdown of syntenin-a in the YSL. Although generally targeted mutagenesis using CRISPR/Cas9 would be the method of choice, the generation of a null allele would not affect maternal contribution of syntenin-a mRNA (Lambaerts et al., 2012) until reaching F3, and maternal-zygotic mutants will likely have too broad effects to address our specific point. While we did initiate the generation of a null line (data not shown), we realized that since exosome secretion from the YSL could be observed as early as 1 dpf, the use of MO injected in the YSL was preferred to (1) be able to affect maternal contribution of syntenin-a mRNA and (2) achieve tissue-specific knockdown of syntenin-a. We are well aware that the application of MO in zebrafish has to be approached with caution, and proper controls are needed to distinguish specific phenotypes from off-target effects, as outlined in recently published guidelines (Stainier et al., 2017). The specific MO we applied has been used in a previous publication and complies with the additional guidelines as recently set out (Lambaerts et al., 2012; Stainier et al., 2017). In addition, we titrated the MO for its ability to sufficiently block exosome secretion while minimizing mortality and performed an additional rescue experiment (Figure S2A). Future studies with syntenin-a KO lines will be indispensable to deepen our understanding of the contribution of this exosome biogenesis pathway to exosome physiology *in vivo* but might require tissue-specific KO.

Importantly, the study of Hyenne et al. (2019) also used zebrafish embryos to investigate the behavior and fate of systemically injected exogenous exosomes originating from zebrafish melanoma cells. Whereas previous studies have indicated how tumor-exosome integrins determine their organotropism (Hoshino et al., 2015), the combination of both models presented here reveals common uptake mechanisms between (exogenous) pathological exosomes and (endogenous) physiological exosomes, an interesting phenotype that has never been explored before at this scale. How circulating EVs target specific cell types at distance remains to be solved, mostly because this step could not be visualized before, but the *in vivo* models presented here pave new avenues to unveil such mechanisms under physiological and pathological conditions. The genetic and structural homologies between zebrafish and human open new perspectives to validate exosome-mediated intercellular communication in the complex architecture of the organism, notably inter-organ communication and their ability to cross biological barriers. The fast development of disease models in zebrafish also provides the opportunity to tackle putative roles of exosomes in several pathologies (Yáñez-Mó et al., 2015), which involves a complex network of cell types. Therefore, the zebrafish

embryo-expressing fluorescent proteins associated with exosomes (e.g., CD63-pHluorin) are a relevant model to study endogenous EVs *in vivo* to unravel fundamental aspects in EV physiology and to assess their clinical applications. Together, our study showcases the variety of questions that could likely be investigated in model organisms to validate the numerous *in vitro* studies on the biology and function of EVs so far.

STAR★METHODS

Detailed methods are provided in the online version of this paper and include the following:

- KEY RESOURCES TABLE
- CONTACT FOR REAGENT AND RESOURCE SHARING
- EXPERIMENTAL MODEL AND SUBJECT DETAILS
  - Zebrafish Strains
  - Cell Lines
- METHOD DETAILS
  - Construction of pUbi-CD63-pHluorin
  - Morpholino Injection
  - Plasmid DNA Injections
  - VLDL Labeling
  - Decreasing Pace-Maker Activity
  - Live Fluorescent Imaging
  - DIC Video-Microscopy/'Nomarski'
  - Electron Microscopy
  - Image Analysis
  - Generation of EV-Heatmap in Zebrafish Embryo
  - Exosome Preparation from *In Vitro* Cultured Cells
  - Exosome Isolation from Zebrafish Embryos
  - NTA Measurements
  - Label-free Mass-Spectrometry
  - Analysis of Growth in the CVP
- QUANTIFICATION AND STATISTICAL ANALYSIS
- DATA AND SOFTWARE AVAILABILITY

SUPPLEMENTAL INFORMATION

Supplemental Information includes two figures, two tables, and six videos and can be found with this article online at https://doi.org/10.1016/j.devcel.2019.01.004.

ACKNOWLEDGMENTS

We acknowledge Vincent Fraisier, Ludovic Leconte, Laetitia Pidial, and Christine Viaris for technical assistance and Karine Duroure and Mylène Lancino for assistance and helpful discussions. The authors greatly acknowledge the Cell and Tissue Imaging (PICT-IBiSA) and Nikon Imaging Centre, Institut Curie, member of the French National Research Infrastructure France-BioImaging (ANR10-INBS-04), the NeurImag imaging platform at the IPNP, and the Zebrafish Platform at Insitut Curie. Financing support has been provided by Fondation pour la Recherche Medicale (contract AJE20160635884) to G.v.N., the European Molecular Biology Organization grant (EMBO ALTF 1383-2014) to F.J.V., the Fondation ARC pour la Recherche sur le Cancer fellowship (PJA 20161204808) to F.J.V., LabEx CelTisPhyBio to G.v.N. and F.J.V., and a "Région Ile-de-France" grant to D.L.

AUTHOR CONTRIBUTIONS

Conceptualization, F.J.V. and G.v.N.; Methodology, F.J.V., G.v.N., F.D.B., and D.M.P.; Validation, F.J.V.; Formal Analysis, F.J.V., G.v.N., G. Arras, and G. Allio; Investigation, F.J.V., C.R., F.D., G.F., and G.v.N.; Resources, F.D.B., P.H., J.G.G., and P.Z.; Data Curation, F.J.V. and G.A.; Writing – Original Draft, F.J.V. and G.v.N.; Writing – Review & Editing, F.J.V., G.v.N., D.M.P., G.R., P.H., F.D.B., C.R., and J.G.G.; Visualization, F.J.V.; Supervision, G.v.N., F.D.B., and D.L.; Project Administration, G.v.N.; Funding Acquisition, F.J.V. and G.v.N.

DECLARATION OF INTERESTS

The authors declare no competing interests.

Received: March 15, 2018
Revised: December 21, 2018
Accepted: December 31, 2018
Published: February 7, 2019

REFERENCES

Allen, T.M., and Cullis, P.R. (2013). Liposomal drug delivery systems: From concept to clinical applications. Adv. Drug Deliv. Rev. *65*, 36–48.

Ashley, J., Cordy, B., Lucia, D., Fradkin, L.G., Budnik, V., and Thomson, T. (2018). Retrovirus-like gag protein Arc1 binds RNA and traffics across synaptic boutons. Cell *172*, 262–274.e11.

Bachy, I., Kozyraki, R., and Wassef, M. (2008). The particles of the embryonic cerebrospinal fluid: how could they influence brain development? Brain Res. Bull. *75*, 289–294.

Baietti, M.F., Zhang, Z., Mortier, E., Melchior, A., Degeest, G., Geeraerts, A., Ivarsson, Y., Depoortere, F., Coomans, C., Vermeiren, E., et al. (2012). Syndecan-syntenin-ALIX regulates the biogenesis of exosomes. Nat. Cell Biol. *14*, 677–685.

Campbell, F., Bos, F.L., Sieber, S., Arias-Alpizar, G., Koch, B.E., Huwyler, J., Kros, A., and Bussmann, J. (2018). Directing nanoparticle biodistribution through evasion and exploitation of Stab2-dependent nanoparticle uptake. ACS Nano *12*, 2138–2150.

Charoenviriyakul, C., Takahashi, Y., Morishita, M., Matsumoto, A., Nishikawa, M., and Takakura, Y. (2017). Cell type-specific and common characteristics of exosomes derived from mouse cell lines: yield, physicochemical properties, and pharmacokinetics. Eur. J. Pharm. Sci. *96*, 316–322.

Christensen, K.A., Myers, J.T., and Swanson, J.A. (2002). PH-dependent regulation of lysosomal calcium in macrophages. J. Cell Sci. *115*, 599–607.

Ellett, F., Pase, L., Hayman, J.W., Andrianopoulos, A., and Lieschke, G.J. (2011). mpeg1 promoter transgenes direct macrophage-lineage expression in zebrafish. Blood. *117*, e49–e56.

EV-TRACK Consortium, Van Deun, J., Mestdagh, P., Agostinis, P., Akay, Ö., Anand, S., Anckaert, J., Martinez, Z.A., Baetens, T., Beghein, E., et al. (2017). EV-TRACK: transparent reporting and centralizing knowledge in extracellular vesicle research. Nat. Methods *14*, 228–232.

Fais, S., O'Driscoll, L., Borras, F.E., Buzas, E., Camussi, G., Cappello, F., Carvalho, J., Cordeiro da Silva, A., Del Portillo, H., El Andaloussi, S., et al. (2016). Evidence-based clinical use of nanoscale extracellular vesicles in nanomedicine. ACS Nano *10*, 3886–3899.

Ferguson, S.M., and De Camilli, P. (2012). Dynamin, a membrane-remodelling GTPase. Nat. Rev. Mol. Cell Biol. *13*, 75–88.

Fukuda, M., Ohtani, K., Jang, S.J., Yoshizaki, T., Mori, K., Motomura, W., Yoshida, I., Suzuki, Y., Kohgo, Y., and Wakamiya, N. (2011). Molecular cloning and functional analysis of scavenger receptor zebrafish CL-P1. Biochim. Biophys. Acta *1810*, 1150–1159.

Gabrusiewicz, K., Li, X., Wei, J., Hashimoto, Y., Marisetty, A.L., Ott, M., Wang, F., Hawke, D., Yu, J., Healy, L.M., et al. (2018). Glioblastoma stem cell-derived exosomes induce M2 macrophages and PD-L1 expression on human monocytes. Oncoimmunology *7*, e1412909.

Galindo-Hernandez, O., Villegas-Comonfort, S., Candanedo, F., González-Vázquez, M.C., Chavez-Ocaña, S., Jimenez-Villanueva, X., Sierra-Martinez, M., and Salazar, E.P. (2013). Elevated concentration of microvesicles isolated from peripheral blood in breast cancer patients. Arch. Med. Res. *44*, 208–214.

Gould, S.J., and Raposo, G. (2013). As we wait: coping with an imperfect nomenclature for extracellular vesicles. J. Extracell. Vesicles *2*, 20389.

Gromov, P., Gromova, I., Olsen, C.J., Timmermans-Wielenga, V., Talman, M.L., Serizawa, R.R., and Moreira, J.M.A. (2013). Tumor interstitial fluid — A treasure trove of cancer biomarkers. Biochim. Biophys. Acta *1834*, 2259–2270.

Harper, C.B., Popoff, M.R., McCluskey, A., Robinson, P.J., and Meunier, F.A. (2013). Targeting membrane trafficking in infection prophylaxis: dynamin inhibitors. Trends Cell Biol. *23*, 90–101.

Helker, C.S.M., Schuermann, A., Karpanen, T., Zeuschner, D., Belting, H.G., Affolter, M., Schulte-Merker, S., and Herzog, W. (2013). The zebrafish common cardinal veins develop by a novel mechanism: lumen ensheathment. Development *140*, 2776–2786.

Hermkens, D.M.A., Duckers, H.J., and Schulte-Merker, S. (2015). Vascular development in the zebrafish. In Endothelial Signaling in Development and Disease, M.H.H. Schmidt and S. Liebner, eds. (Springer), pp. 47–64.

Hoshino, A., Costa-Silva, B., Shen, T.-L., Rodrigues, G., Hashimoto, A., Tesic Mark, M., Molina, H., Kohsaka, S., Di Giannatale, A., Ceder, S., et al. (2015). Tumour exosome integrins determine organotropic metastasis. Nature *527*, 329–335.

Hurbain, I., Geerts, W.J., Boudier, T., Marco, S., Verkleij, A.J., Marks, M.S., and Raposo, G. (2008). Electron tomography of early melanosomes: implications for melanogenesis and the generation of fibrillar amyloid sheets. Proc. Natl. Acad. Sci. U S A. *105*, 19726–31.

Hyenne, V., Ghoroghi, S., Collot, M., Bons, J., Follain, G., Harlepp, S., Mary, B., Bauer, J., Mercier, L., Busnelli, I., et al. (2019). Studying the fate of tumor extracellular vesicles at high spatiotemporal resolution using the zebrafish embryo. Dev. Cell *48*. Published online February 7, 2019. https://doi.org/10.1016/j.devcel.2019.01.014.

Hyenne, V., and Goetz, J.G. (2017). Extracellular vesicles on the wire. Cell Adh. Migr. *11*, 121–123.

Imai, T., Takahashi, Y., Nishikawa, M., Kato, K., Morishita, M., Yamashita, T., Matsumoto, A., Charoenviriyakul, C., and Takakura, Y. (2015). Macrophage-dependent clearance of systemically administered B16BL6-derived exosomes from the blood circulation in mice. J. Extracell. Vesicles *4*, 26238.

Jang, S., Ohtani, K., Fukuoh, A., Mori, K., Yoshizaki, T., Kitamoto, N., Kim, Y., Suzuki, Y., and Wakamiya, N. (2014). Scavenger receptor CL-P1 mediates endocytosis by associating with AP-2μ2. Biochim. Biophys. Acta *1840*, 3226–3237.

Jenne, C.N., and Kubes, P. (2013). Immune surveillance by the liver. Nat. Immunol. *14*, 996–1006.

Jin, S.W., Beis, D., Mitchell, T., Chen, J.N., and Stainier, D.Y. (2005). Cellular and molecular analyses of vascular tube and lumen formation in zebrafish. Development. *132*, 5199–5209.

Johnstone, R.M., Bianchini, A., and Teng, K. (1989). Reticulocyte maturation and exosome release: transferrin receptor containing exosomes shows multiple plasma membrane functions. Blood *74*, 1844–1851.

Kowal, J., Arras, G., Colombo, M., Jouve, M., Morath, J.P., Primdal-Bengtson, B., Dingli, F., Loew, D., Tkach, M., and Théry, C. (2016). Proteomic comparison defines novel markers to characterize heterogeneous populations of extracellular vesicle subtypes. Proc. Natl. Acad. Sci. USA *113*, E968–E977.

Lai, C.P., Kim, E.Y., Badr, C.E., Weissleder, R., Mempel, T.R., Tannous, B.A., and Breakefield, X.O. (2015). Visualization and tracking of tumour extracellular vesicle delivery and RNA translation using multiplexed reporters. Nat. Commun. *6*, 7029.

Lambaerts, K., Van Dyck, S., Mortier, E., Ivarsson, Y., Degeest, G., Luyten, A., Vermeiren, E., Peers, B., David, G., and Zimmermann, P. (2012). Syntenin, a syndecan adaptor and an Arf6 phosphatidylinositol 4,5-bisphosphate effector, is essential for epiboly and gastrulation cell movements in zebrafish. J. Cell Sci. *125*, 1129–1140.

Lenard, A., Ellertsdottir, E., Herwig, L., Krudewig, A., Sauteur, L., Belting, H.G., and Affolter, M. (2013). In vivo analysis reveals a highly stereotypic morphogenetic pathway of vascular anastomosis. Dev Cell. *25*, 492–506.

Lo Cicero, A., Stahl, P.D., and Raposo, G. (2015). Extracellular vesicles shuffling intercellular messages: for good or for bad. Curr. Opin. Cell Biol. *35*, 69–77.

Logozzi, M., De Milito, A., Lugini, L., Borghi, M., Calabrò, L., Spada, M., Perdicchio, M., Marino, M.L., Federici, C., Iessi, E., et al. (2009). High levels of exosomes expressing CD63 and caveolin-1 in plasma of melanoma patients. PLoS One *4*, e5219.

Lysko, P.G., Weinstock, J., Webb, C.L., Brawner, M.E., and Elshourbagy, N.A. (1999). Identification of a small-molecule, nonpeptide macrophage scavenger receptor antagonist. J. Pharmacol. Exp. Ther. *289*, 1277–1285.

McGough, I.J., and Vincent, J.P. (2016). Exosomes in developmental signalling. Development *143*, 2482–2493.

Miyares, R.L., de Rezende, V.B., and Farber, S.A. (2014). Zebrafish yolk lipid processing: a tractable tool for the study of vertebrate lipid transport and metabolism. Dis. Model. Mech. *7*, 915–927.

Mosimann, C., Kaufman, C.K., Li, P., Pugach, E.K., Tamplin, O.J., and Zon, L.I. (2011). Ubiquitous transgene expression and Cre-based recombination driven by the ubiquitin promoter in zebrafish. Development. *138*, 169–177.

Murayama, E., Kissa, K., Zapata, A., Mordelet, E., Briolat, V., Lin, H.F., Handin, R.I., and Herbomel, P. (2006). Tracing hematopoietic precursor migration to successive hematopoietic organs during zebrafish development. Immunity *25*, 963–975.

Naegeli, K.M., Hastie, E., Garde, A., Wang, Z., Keeley, D.P., Gordon, K.L., Pani, A.M., Kelley, L.C., Morrissey, M.A., Chi, Q., et al. (2017). Cell invasion in vivo via rapid exocytosis of a transient lysosome-derived membrane domain. Dev. Cell *43*, 403–417.e10.

van Niel, G., D'Angelo, G., and Raposo, G. (2018). Shedding light on the cell biology of extracellular vesicles. Nat. Rev. Mol. Cell Biol. *19*, 213–228.

Pastuzyn, E.D., Day, C.E., Kearns, R.B., Kyrke-Smith, M., Taibi, A.V., McCormick, J., Yoder, N., Belnap, D.M., Erlendsson, S., Morado, D.R., et al. (2018). The neuronal gene arc encodes a repurposed retrotransposon gag protein that mediates intercellular RNA transfer. Cell *172*, 275–288.

Plebanek, M.P., Mutharasan, R.K., Volpert, O., Matov, A., Gatlin, J.C., and Thaxton, C.S. (2015). Nanoparticle targeting and cholesterol flux Through scavenger receptor Type B-1 inhibits cellular exosome uptake. Sci. Rep. *5*, 15724.

Poisson, J., Lemoinne, S., Boulanger, C., Durand, F., Moreau, R., Valla, D., and Rautou, P.E. (2017). Liver sinusoidal endothelial cells: physiology and role in liver diseases. J. Hepatol. *66*, 212–227.

Poullet, P., Carpentier, S., and Barillot, E. (2007). myProMS, a web server for management and validation of mass spectrometry-based proteomic data. Proteomics *7*, 2553–2556.

Poynter, S.J., Weleff, J., Soares, A.B., and DeWitte-Orr, S.J. (2015). Class-A scavenger receptor function and expression in the rainbow trout (Oncorhynchus mykiss) epithelial cell lines RTgutGC and RTgill-W1. Fish Shellfish Immunol. *44*, 138–146.

Raiborg, C., Wenzel, E.M., Pedersen, N.M., Olsvik, H., Schink, K.O., Schultz, S.W., Vietri, M., Nisi, V., Bucci, C., Brech, A., et al. (2015). Repeated ER–endosome contacts promote endosome translocation and neurite outgrowth. Nature *520*, 234–238.

Raposo, G., Tenza, D., Murphy, D.M., Berson, J.F., and Marks, M.S. (2001). Distinct protein sorting and localization to premelanosomes, melanosomes, and lysosomes in pigmented melanocytic cells. J. Cell Biol. *152*, 809–824.

Seternes, T., Sørensen, K., and Smedsrød, B. (2002). Scavenger endothelial cells of vertebrates: a nonperipheral leukocyte system for high-capacity elimination of waste macromolecules. Proc. Natl. Acad. Sci. USA *99*, 7594–7597.

Stainier, D.Y.R., Raz, E., Lawson, N.D., Ekker, S.C., Burdine, R.D., Eisen, J.S., Ingham, P.W., Schulte-Merker, S., Yelon, D., Weinstein, B.M., et al. (2017). Guidelines for morpholino use in zebrafish. PLoS Genet. *13*, e1007000.

Sung, B.H., Ketova, T., Hoshino, D., Zijlstra, A., and Weaver, A.M. (2015). Directional cell movement through tissues is controlled by exosome secretion. Nat. Commun. *6*, 7164.

Théry, C., Amigorena, S., Raposo, G., and Clayton, A. (2006). Isolation and characterization of exosomes from cell culture supernatants and biological fluids. Curr. Protoc. Cell Biol. *3*, 22.

Thomou, T., Mori, M.A., Dreyfuss, J.M., Konishi, M., Sakaguchi, M., Wolfrum, C., Rao, T.N., Winnay, J.N., Garcia-Martin, R., Grinspoon, S.K., et al. (2017). Adipose-derived circulating miRNAs regulate gene expression in other tissues. Nature *542*, 450–455.

Tian, T., Wang, Y., Wang, H., Zhu, Z., and Xiao, Z. (2010). Visualizing of the cellular uptake and intracellular trafficking of exosomes by live-cell microscopy. J. Cell. Biochem. *111*, 488–496.

Tkach, M., and Théry, C. (2016). Communication by extracellular vesicles: where we are and where we need to go. Cell *164*, 1226–1232.

Trajkovic, K., Hsu, C., Chiantia, S., Rajendran, L., Wenzel, D., Wieland, F., Schwille, P., Brügger, B., and Simons, M. (2008). Ceramide triggers budding of exosome vesicles into multivesicular endosomes. Science *319*, 1244–1247.

Valot, B., Langella, O., Nano, E., and Zivy, M. (2011). MassChroQ: a versatile tool for mass spectrometry quantification. Proteomics *11*, 3572–3577.

Vermot, J., Forouhar, A.S., Liebling, M., Wu, D., Plummer, D., Gharib, M., and Fraser, S.E. (2009). Reversing blood flows act through klf2a to ensure normal valvulogenesis in the developing heart. PLoS Biol. *7*, e1000246.

Verweij, F.J., Bebelman, M.P., Jimenez, C.R., Garcia-Vallejo, J.J., Janssen, H., Neefjes, J., Knol, J.C., de Goeij-de Haas, R., Piersma, S.R., et al. (2018). Quantifying exosome secretion from single cells reveals a modulatory role for GPCR signaling. J Cell Biol. *217*, 1129–1142.

Vizcaíno, J.A., Deutsch, E.W., Wang, R., Csordas, A., Reisinger, F., Ríos, D., Dianes, J.A., Sun, Z., Farrah, T., Bandeira, N., et al. (2014). ProteomeXchange provides globally coordinated proteomics data submission and dissemination. Nat. Biotechnol. *32*, 223–226.

Walzer, C., and Schönenberger, N. (1979). Ultrastructure and cytochemistry of the yolk syncytial layer in the alevin of trout (Salmo fario trutta L. and Salmo gairdneri R.) after hatching. II. The cytoplasmic zone. Cell Tissue Res. *196*, 75–93.

Westerfield, M. (2000). The Zebrafish Book. A Guide for the Laboratory Use of Zebrafish (Danio rerio) (University of Oregon Press).

White, R.M., Sessa, A., Burke, C., Bowman, T., LeBlanc, J., Ceol, C., Bourque, C., Dovey, M., Goessling, W., Burns, C.E., and Zon, L.I. (2008). Transparent adult zebrafish as a tool for in vivo transplantation analysis. Cell Stem Cell. *2*, 183–189.

Wiklander, O.P.B., Nordin, J.Z., O'Loughlin, A., Gustafsson, Y., Corso, G., Mäger, I., Vader, P., Lee, Y., Sork, H., Seow, Y., et al. (2015). Extracellular vesicle in vivo biodistribution is determined by cell source, route of administration and targeting. J. Extracell. Vesicles *4*, 26316.

Yáñez-Mó, M., Siljander, P.R., Andreu, Z., Zavec, A.B., Borràs, F.E., Buzas, E.I., Buzas, K., Casal, E., Cappello, F., Carvalho, J., et al. (2015). Biological properties of extracellular vesicles and their physiological functions. J. Extracell. Vesicles *4*, 27066.

Yao, Y., Jones, E., and Inoki, K. (2017). Lysosomal regulation of mTORC1 by amino acids in mammalian cells. Biomolecules *7*, 51.

Yim, N., Ryu, S.W., Choi, K., Lee, K.R., Lee, S., Choi, H., Kim, J., Shaker, M.R., Sun, W., Park, J.H., et al. (2016). Exosome engineering for efficient intracellular delivery of soluble proteins using optically reversible protein–protein interaction module. Nat. Commun. *7*, 12277.

Yoshimura, A., Kawamata, M., Yoshioka, Y., Katsuda, T., Kikuchi, H., Nagai, Y., Adachi, N., Numakawa, T., Kunugi, H., Ochiya, T., et al. (2016). Generation of a novel transgenic rat model for tracing extracellular vesicles in body fluids. Sci. Rep. *6*, 31172.

Zomer, A., Maynard, C., Verweij, F.J., Kamermans, A., Schäfer, R., Beerling, E., Schiffelers, R.M., de Wit, E., Berenguer, J., Ellenbroek, S.I.J., et al. (2015). In vivo imaging reveals extracellular vesicle-mediated phenocopying of metastatic behavior. Cell *161*, 1046–1057.

STAR★METHODS

KEY RESOURCES TABLE

REAGENT or RESOURCE	SOURCE	IDENTIFIER
Antibodies		
Rabbit anti-GFP	Molecular Probes	Cat# A-11122; RRID: AB_221569
GFP-trap	ChromoTek	Cat# gtma-20; RRID: AB_2631358
Chemicals, Peptides, and Recombinant Proteins		
Lidocaine	Sigma-Aldrich	L7757
Tricaine	Sigma-Aldrich	MS-222
Bafilomycin-A1	Sigma-Aldrich	SML1661
Dextran Sulfate 500 kDa	Sigma-Aldrich	D8906
BODIPY C12 558/568	Life Technologies SAS	D3835
Collagenase I	ThermoFisher	17018029
25% glutaraldehyde	EMS	16220
Cacodylate 100 g	EMS	12300
Osmium 4%	EMS	19170
PFA	EMS	15710
Phosphate buffer (NaH2PO4)	Sigma-Aldrich	S8282
EPON	TAAB	T024
Deposited Data		
Proteomics data	PRIDE Repository	PXD011258
EV related experimental details	EV-track consortium	EV180009
Experimental Models: Organisms/Strains		
Zebrafish: Casper	White et al., 2008	N/A
Zebrafish: *kdrl:Hsa.HRAS-mCherry* : Tg(kdrl:Hsa.HRAS-mCherry)s916	Stainier lab	ZFIN: ZDB-ALT-090506-2
Zebrafish: *mpeg1:mCherryF* : Tg(mpeg1:mCherryF)	Ellett et al., 2011	ZFIN: ZDB-ALT-120117-2
Zebrafish: *kdrl:EGFP* : Tg(kdrl:EGFP)	Stainier lab; Jin et al., 2005	ZFIN: ZDB-ALT-061120-6
Zebrafish: *kdrl:nls-mKate2* : Tg(kdrl:nls-mKate2)	Lenard et al., 2013	ZFIN: ZDB-FISH-150901-2655
Oligonucleotides		
Primers for cloning CD63-pHluorin into pDONR221 For 5'-GGGGACAAGTTTGTACAAAAAAGCAGGCTGGatggcggtgga aggagga-3' Rev 5'-GGGGACCACTTTGTACAAGAAAGCTGGGTCctacatcacctc gtagccacttct-3'	This paper	N/A
zSyntenin-A Morpholino (SyntA MO) 5'-TACAACGACATCCTTTCT GCTTTCA-3'	Lambaerts et al., 2012	N/A
Ctrl Morpholino (Ctrl MO) 5'- CCTCTTACCTCAGTTACAATTTATA-3'	Gene Tools	PCO-StandardControl-100
Recombinant DNA		
pCMV-CD63-pHluorin	Verweij et al., 2018	N/A
pDONR221	Invitrogen	N/A (Gateway)
p5E-ubi	Mosimann et al., 2011 Addgene	27320
p3E-polyA 153	Invitrogen	N/A (Gateway)
pCS2-zSyntenin-a wt 83-11	Zimmermann lab/this paper	1561
pDEST R4-R3	Invitrogen	N/A (Gateway)
pUbi-CD63-pHluorin	this paper	N/A
Software and Algorithms		
Fiji / ImageJ	NIH	RRID:SCR_002285
Metamorph	Molecular Devices	N/A
GraphPad PRISM	GraphPad Software	N/A

(*Continued on next page*)

Continued

REAGENT or RESOURCE	SOURCE	IDENTIFIER
Other		
Polypropylene centrifuge tubes, 11 x 34 mm	Beckman Coulter	347287
Polypropylene centrifuge tubes, 25 x 89 mm	Beckman Coulter	326823

CONTACT FOR REAGENT AND RESOURCE SHARING

Further information and requests for resources and reagents should be directed to and will be fulfilled by the Lead Contact, Guillaume van Niel (guillaume.van-niel@inserm.fr).

EXPERIMENTAL MODEL AND SUBJECT DETAILS

Zebrafish Strains

Zebrafish were staged and cared for according to standard protocols (Westerfield, 2000). All fish are housed in the fish facility of our laboratory, which was built according to the local animal welfare standards. All animal procedures were performed in accordance with French and European Union animal welfare guidelines. We performed our analyses at 3 dpf. At this developmental stage, sex ratios cannot be determined (gonad differentiation begins around 25 dpf). Adult density was maintained at ~7-8 fish/L, and fish were fed twice daily with artemia and dry food (SDS-400, DIETEX France). Water temperature was maintained at 28°C.

Cell Lines

AB.9 (ATCC CRL-2298) cells are fibroblast obtained from the caudal fin of an adult AB strain zebrafish. AB.9 cultures were grown in Leibovitz-L15 CO_2-independent medium supplemented with 15% heat-inactivated bovine serum at 28°C and passaged when reaching 90% confluency (1-2 times/week).

METHOD DETAILS

Construction of pUbi-CD63-pHluorin

pUbi-CD63-pHluorin was constructed by first cloning CD63-pHluorin (human CD63; sequence identical to Verweij et al., 2018) using primer pairs 5'-GGGGACAAGTTTGTACAAAAAAGCAGGCTGGatggcggtggaaggagga-3' (fwd) and 5'-GGGGACCACTTTGTACAAGAAAGCTGGGTCctacatcacctcgtagccacttct-3' (rev) into pDONR221 (Gateway, Invitrogen). pDONR221-CD63-pHluorin was subsequently recombined with p5E-ubi (Addgene plasmid # 27320), p3E-polyA 153, and pDEST R4-R3 (Gateway, Invitrogen) to create pUbi-CD63-pHluorin.

Morpholino Injection

The MO against zSyntenin-A, and Standard Control oligo were purchased from GeneTools, used at 1:4 dilution from a 1 mM stock, and injected at 0.5-1.0 nL. The Synt-a MO has been previously validated for its effect on the YSL (Lambaerts et al., 2012). To minimize potential off-targets effects in the current study, the optimal MO concentration for YSL-injection was titrated as the minimal concentration causing the studied phenotype while minimizing mortality or phenotypic abnormalities compared to control.

Plasmid DNA Injections

To induce expression of CD63-pHluorin, embryos were injected at the one-cell stage (for ubiquitous expression) or at 4h in the YSL (for YSL-specific expression). On the next day, injected embryos were inspected under a stereomicroscope. Only embryos that developed normally were assayed.

VLDL Labeling

BODIPY C12 was dissolved in canola oil as lipid (slow release) carrier at 1.5 μg/μl; approximately 5nl was injected in the yolk per embryo.

Decreasing Pace-Maker Activity

Lidocaine was dissolved in ethanol and used at 640μM. After 2h incubation, zebrafish pace-maker activity was assessed by recording the heart-beat for 20 seconds at high speed (30Hz) using a video microscope with stage incubator maintained at 28°C.

Live Fluorescent Imaging

Embryos were anesthetized with tricaine and embedded in 1.5% low melting point agarose. For most experiments, embryos were imaged at 3 dpf. Recordings were performed at 28°C using a Nikon TSi spinning-wide (Yokagawa CSU-W1) microscope, equipped with a 60x CFI Plan Apo IR SR W NA 1.27, a sCMOS 1200x1200 Prime95B from Photometrics (pixel size:11 μm) and a sCMOS 2048x2048 Orca Flash 4 v2 from Hamamatsu (pixel size:6.5 μm).

DIC Video-Microscopy/'Nomarski'

Embryos were examined with a Reichert Polyvar 2 microscope with DIC optics and equipped with a Hitachi HV-C20 tri-CCD camera. All contrast-dampening functions were set off, so that with the ×100 (oil immersion) objective, the final magnification on a 26-cm video screen was ×4000 with excellent contrast, such that mitochondria and intracellular vesicle trafficking could be observed. Video-sequences were recorded from the Y/C output of the camera by a Sony DHR1000 tape recorder in Digital Video (DV) format. Single video images were captured and stored on a PC from the DV videotapes, through the Sony DVK2000 capture board.

Electron Microscopy

For conventional EM, Zebrafish embryos 3 dpf were fixed in 2.5% glutaraldehyde in 0.1 M cacodylate buffer for 24 h, post-fixed with 1% osmium tetroxide, dehydrated in ethanol and embedded in epon as described (Raposo et al., 2001). Epon embedding was performed as described (Hurbain et al., 2008). Ultrathin sections of zebrafish were prepared with a Reichert UltracutS ultramicrotome (Leica Microsystems) and contrasted with uranyl acetate and lead citrate.

For ultrathin cryosectioning and immunogold labeling, zebrafish were fixed in 2% PFA, 0.2% glutaraldehyde in 0.1M phosphate buffer pH 7.4. Zebrafishes were processed for ultracryomicrotomy and immunogold labeled using PAG 10 as described (Raposo et al., 2001).

Exosome pellets were deposited on carbonated grids and fixed in 2% PFA in 0.1 M phosphate buffer, pH 7.4. The grids were then processed for single immunogold labeled using PAG10 (Raposo et al., 2001) and embedded in methyl-cellulose Uranyl Acetate 0,4%.

All samples were examined with a FEI Tecnai Spirit electron microscope (FEI Company), and digital acquisitions were made with a numeric camera (Quemesa; Soft Imaging System).

Image Analysis

All imaging data was analyzed using ImageJ. Mander's overlap coefficient was determined using the JACoP plugin.

Generation of EV-Heatmap in Zebrafish Embryo

The heatmap was generated using Fiji and MATLAB software. After image acquisition, the particles (immobilized EVs at the endothelial walls) were identified after analyses of the z-stacks with Fiji for each fish. The positions of these events were registered on a gray-level support image of a 3 dpf zebrafish plexus by drawing dots at the position of the events. Next, all support images were put together in a z-stack, one layer corresponding to each fish. The next step was to read this support-image z-stack layer by layer with MATLAB, where the dots representing the particles were automatically detected with the function HoughCircles (Yuan-Liang Tang, Department of Information Management, Chaoyang University of Technology, Taichung, Taiwan) using the Circular Hough Transform based algorithm, giving the coordinates of the detected dots as output. Gaussian spots were then created at these coordinates, with an amplitude of each spot equal to 1. A sum projection of the different layers was generated, after which a black and white mask created with the gray level support image was applied to this sum projection. The gaussian spot amplitudes of each layers were summed to produce the heatmap. The areas of the sum projection where the gaussian spot amplitudes are higher corresponds to high density areas of events. To produce the final heatmap, a custom colormap, inspired by the jet colormap, was applied to the sum projection. The colormap goes from black (no event) to red (high density areas).

Exosome Preparation from *In Vitro* Cultured Cells

Exosomes were prepared from the supernatant of 24h cultured AB.9 cells as described before (Théry et al., 2006). Briefly, exosomes were purified from the cultured media with exosome-free serum. Differential centrifugations at 500 x g (2 x 10 min) and 2,000 x g (2 x 15min) were carried out in a standard lab culture centrifuge using 50mL tubes. Subsequent steps were carried out in an ultracentrifuge, using polyallomer tubes listed above. The 10,000 x g (2 x 30min) steps eliminated cellular debris and centrifugation at 100,000 x g (60 min) pelleted exosomes. The exosome pellet was washed once in a PBS, centrifuged at 100,000 x g for 1 h and re-suspended in 50-200 μL PBS, depending on the starting volume.

Exosome Isolation from Zebrafish Embryos

50 zebrafish embryos 3 dpf were anesthetized and with Collagenase I, used at a concentration 200mg/mL in a total volume of 500μl. Sample was incubated at 29°C for 30-45 min under slow agitation on a heating block, while the sample was intermittently triturated with a sterile 200μl tip, every 10 minutes until large clumps disappeared. EDTA was added to stop the Collagenase activity. The final volume was adjusted to 1mL, and transferred to 11 x 34 mm centrifuge tubes.

Differential centrifugations at 500 g (2 x 10 min), 2,000 g (2 x 15min), 10,000g (2 x 30min) eliminated cellular debris and centrifugation at 100,000 g (60 min) pelleted exosomes. The exosome pellet was washed once in a PBS, centrifuged at 100,000 g for 1 h and re-suspended in 50-200 μL PBS, depending on the starting volume.

NTA Measurements

For NTA measurements of EV-size and concentration, concentrated samples were pre-diluted 2000x, and analyzed using a Nanosight (LM10). Samples were measured at 5 different positions in the chamber for 1 min each, with stage temperature control set at 27°C. The videos were then processed by the Nanosight software (NTA 3.2 Dev Build 3.2.16).

Label-free Mass-Spectrometry

Exosomes were purified by differential ultracentrifugation as described above, and followed (for YSL derived exosomes) by an IP for GFP using GFP-trap magnetic agarose beads (Chromotek). Pull-downs were performed in biological replicates (n = 3) under agitation overnight at 4°C.

To characterize the exosome proteins, we qualitatively and quantitatively analyzed them by Orbitrap Fusion Tribrid mass spectrometry, by using a label free approach. For exosome quantification, SDS/PAGE was used without separation as a clean-up step, and only one gel slice was excised otherwise proteins were separated on SDS/PAGE and four gel slices were excised. Subsequently, gel slices were washed and proteins were reduced with 10 mM DTT before alkylation with 55 mM iodoacetamide. After washing and shrinking the gel pieces with 100% MeCN, we performed in-gel digestion using trypsin/LysC (Promega) overnight in 25 mM NH4HCO3 at 30°C. Peptide were then extracted using 60/35/5 MeCN/H2O/HCOOH and vacuum concentrated to dryness

Samples were chromatographically separated using an RSLCnano system (Ultimate 3000, Thermo Scientific) coupled to an Orbitrap Fusion Tribrid mass spectrometer (Thermo Scientific).

Peptides were loaded onto a C18 column (75-μm inner diameter × 2 cm; nanoViper Acclaim PepMapTM 100 or 300 μm x 5 mm PepMapTM 100, 5 μm, Thermo Scientific), separated and MS data acquired using Xcalibur software. Peptides separation was performed over a linear gradient of 100 min from 5% to 25% or 5% to 35% MeCN (75-μm inner diameter × 50 cm; nanoViper C18, 2 μm or 5 μm, 100Å, Acclaim PepMapTM RSLC, Thermo Scientific). Full-scan MS was acquired in the Orbitrap analyzer with a resolution set to 120,000 and ions from each full scan were HCD fragmented and analyzed in the linear ion trap.

For identification the data were searched against the UniProtKB Zebrafish database using Sequest through proteome discoverer. Enzyme specificity was set to trypsin and a maximum of two missed cleavage site were allowed. Oxidized methionine, N-terminal acetylation, and carbamidomethyl cysteine were set as variable modifications. Maximum allowed mass deviation was set to 10 ppm for monoisotopic precursor ions and 0.6 Da for MS/MS peaks. The resulting files were further processed using myProMS (Poullet et al., 2007). FDR calculation used Percolator and was set to 1%. The label free quantification was performed by peptide Extracted Ion Chromatograms (XICs) computed with MassChroQ version 1.2.1 (Valot et al., 2011). Global MAD normalization was applied on the total signal to correct the XICs for each biological replicate. Protein ratios were computed as the geometrical mean of related peptides. To estimate ratio significance, a two-tailed t test was performed and p values were adjusted with a Benjamini–Hochberg FDR procedure with a control threshold set to 0.05. Fold change-based GO enrichment analysis was performed as in Kowal et al. (Kowal et al., 2016).

Analysis of Growth in the CVP

For height measurements, the longest distance through the z-stack was used, obtained by maximum projection in z and using a fixed point (second ISV from the right). For measurements of the (relative) surface area increase, likewise a maximum projection in z was used and compared over time. To measure proliferation, the number of nuclei were counted at different time points. As a slight mosaicism of the kdrl:nls-mKate2 line could not be fully excluded, we expressed proliferation relative to the control.

QUANTIFICATION AND STATISTICAL ANALYSIS

We performed statistical analysis (Student's two-tailed t test for significance) using GraphPad Prism version 6.0 (GraphPad software). Unpaired analysis was used unless specified otherwise. Data distribution was assumed to be normal but this was not formally tested. Sample sizes, statistical test and P values are indicated in the figures or figure legends.

DATA AND SOFTWARE AVAILABILITY

The mass spectrometry proteomics data have been deposited to the ProteomeXchange Consortium (Vizcaíno et al., 2014) via the PRIDE partner repository with the dataset identifier PXD011258. We have submitted all relevant data of our experiments to the EV-TRACK knowledgebase (EV-TRACK ID: EV180009) (Van Deun et al., 2017).

Developmental Cell, Volume *48*

Supplemental Information

Live Tracking of Inter-organ Communication by Endogenous Exosomes *In Vivo*

Frederik J. Verweij, Celine Revenu, Guillaume Arras, Florent Dingli, Damarys Loew, D. Michiel Pegtel, Gautier Follain, Guillaume Allio, Jacky G. Goetz, Pascale Zimmermann, Philippe Herbomel, Filippo Del Bene, Graça Raposo, and Guillaume van Niel

SUPPLEMENTAL INFORMATION to Verweij et al., Live tracking of inter-organ communication by endogenous exosomes in vivo

SUPP FIG 1 - Related to Figures 1 & 2

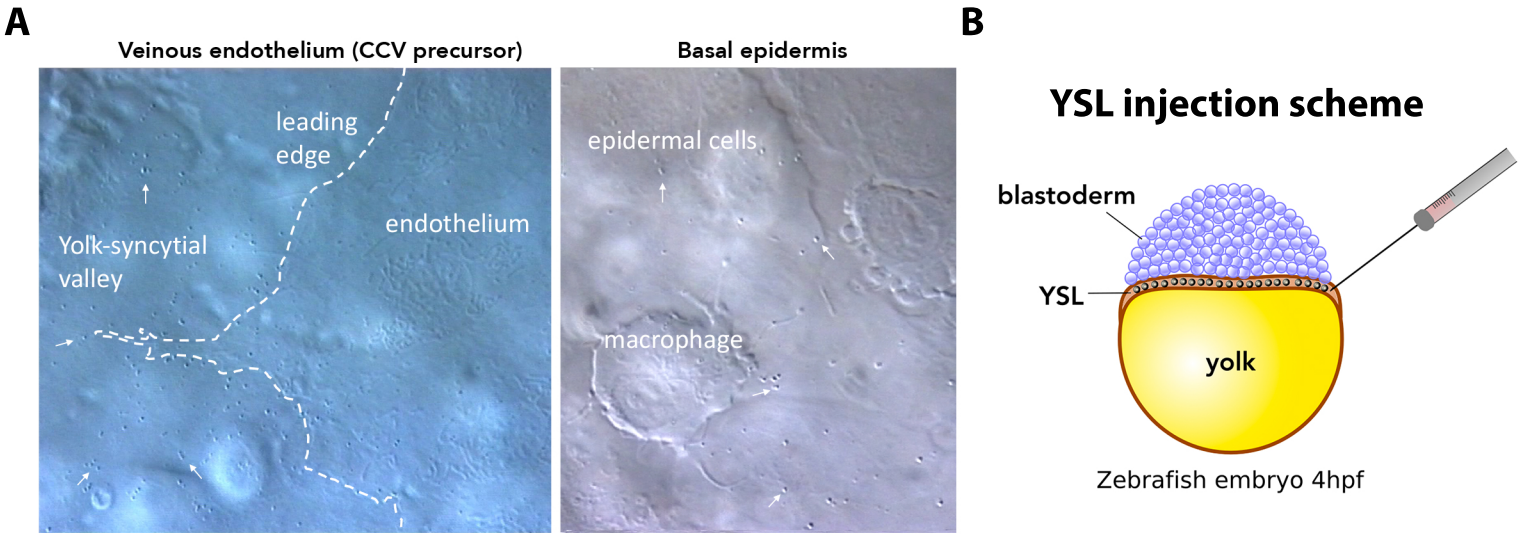

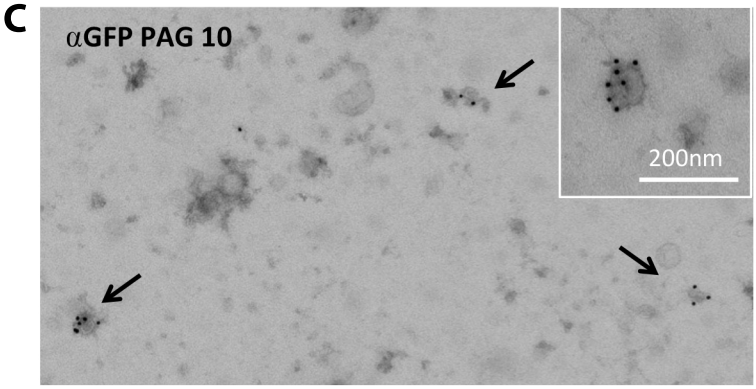

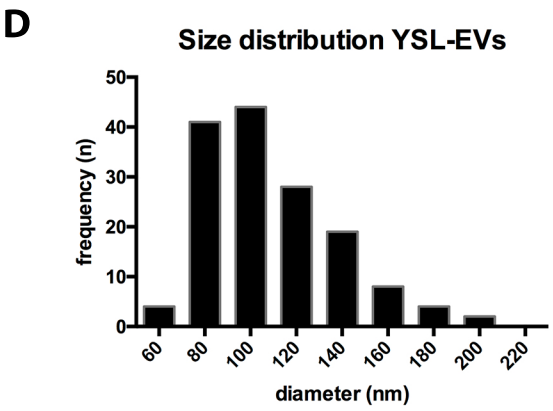

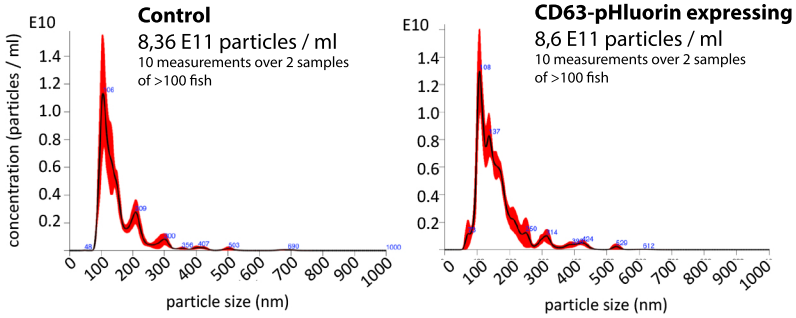

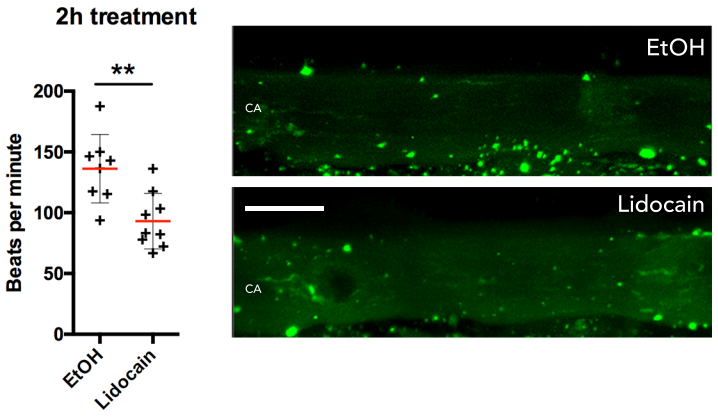

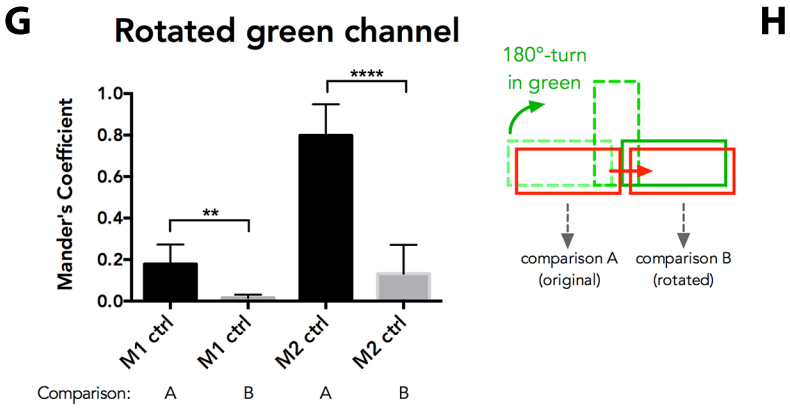

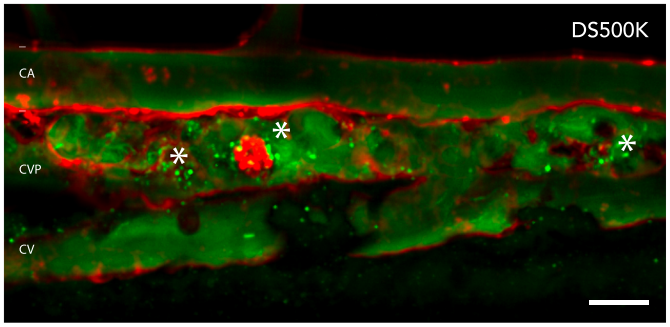

Sup Figure 1 | Related to: Figures 1 & 2 (A) Video-enhanced Nomarski microscopy of the large interstitial space between the YSL and the overlying epidermis around the onset of blood circulation (~24hpf) of a zebrafish embryo, showing numerous extracellular vesicles indicated by white arrows. (B) Schematic of YSL injection at 1000 cells stage. (C) EM analysis on vesicles isolated from dissociated YSL CD63-pHluorin expressing 3dpf zebrafish embryos, labelled with gold particles (PAG10) directed to GFP. (D) Size-distribution of 150 vesicles on the YSL (related to Fig 3C). (E) NTA-analysis of particle concentration on vesicles isolated from dissociated control (left) and YSL CD63-pHluorin expressing fish (right). (F) Effect of blood flow manipulation on attachment of EVs to the CA. To the left: graph showing effect of lidocaine on heart-beat (pacemaker activity) (**$p \leq 0.01$; $n = 8$; unpaired t-test with equal SD). To the right: representative example of EV accumulation in treated (Lidocain) condition and control (EtOH) condition. (G) As in Fig6 B, but with 180-degree rotation of green channel to control for random overlap (mean ± SD; ****$p \leq 0.0001$; $n \geq 3$; unpaired t-test with equal SD). (H) Close-up of the CVP area of 3dpf *Tg(kdrl:Hsa.HRAS-mCherry)* zebrafish embryos expressing CD63-pHluorin in the YSL and pre-incubated with DS500K (-4h) and BafA (-1h) prior to analysis. Asterisks indicate macrophages. Scalebars indicate 10 µm.

SUPP FIG 2 - Related to figure 7

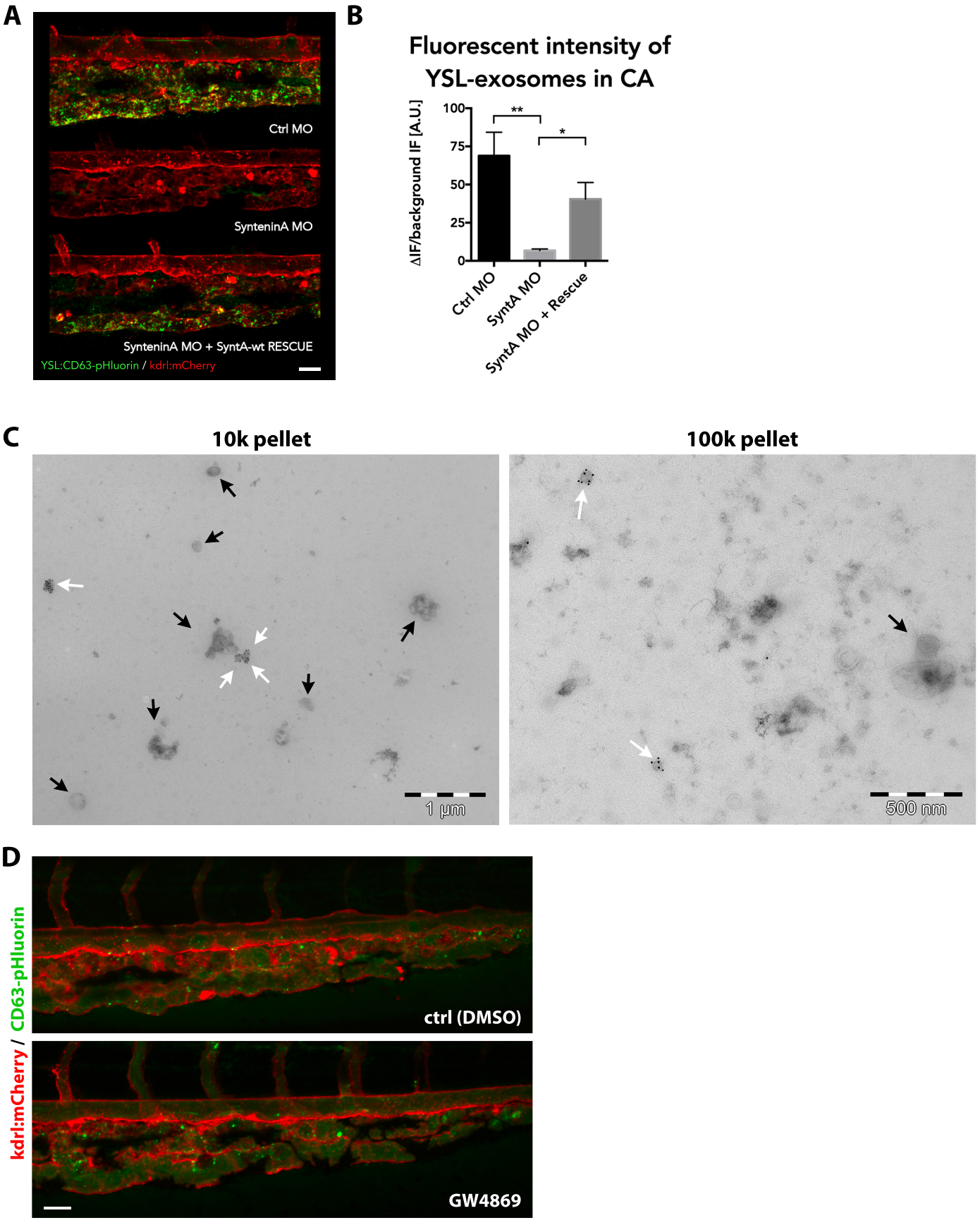

Sup Figure 2 | Related to: Fig 7 (A) Close-up of the CVP area of 3dpf *Tg(kdrl:Hsa.HRAS-mCherry)* zebrafish embryos expressing CD63-pHluorin in the YSL and injected with ctrl (Ctrl MO) (top), Syntenin-a (SynteninA MO) (middle), or Syntenin-a (SynteninA MO) + wt-Syntenin-a plasmid insensitive for SynteninA MO (bottom). (B) Quantification of fluorescent intensity in CA as in Fig7E for experiment shown in (A) (mean ± SD; *$p \leq 0.05$; **$p \leq 0.01$; n = 4; unpaired t-test with equal SD). (C) Electron microscopy image of 10,000g (left panel) and 100,000g pellets (right panel) isolated from dissociated YSL CD63-pHluorin expressing 3dpf zebrafish embryos, labelled with gold particles (PAG10) directed to GFP, showing vesicles with different sizes. White arrows indicate vesicles <150nm, black arrows indicate vesicles >150nm. (D) Overview of the CVP area of a 3dpf Tg(kdrl:Hsa.HRAS-mCherry) zebrafish embryo expressing CD63-pHluorin in the YSL, incubated with GW4869 or DMSO (ctrl) treated. Scalebars indicate 10 µm.